



University Institute of Lisbon

Department of Information Science and Technology

Study and Implementation of an Advanced Transceiver for 5G

Diogo Roque Mendes

A dissertation presented in partial fulfillment of the requirements for the degree
of

Master in Telecommunications and Computer Engineering

Supervisor

Dr. Francisco António Bucho Cercas, Full Professor
ISCTE-IUL

Co-Supervisor

Dr. Adolfo da Visitação Tregreira Cartaxo, Full Professor
ISCTE-IUL

October 2019

"I have not failed. I've just found 10,000 ways that won't work."

THOMAS A. EDISON

Resumo

A quinta geração de redes móveis prevê a concretização de ritmos binários acima de 1 Gbps ao acesso de qualquer utilizador comum. Para concretizar esse requisito, foi necessário levar a cargo um estudo e desenvolvimento de um sistema que utilize a forma de onda do 4^a Geração de Comunicações Móveis (4G) para diminuir eventuais necessidades de adição de novos módulos e aumento da complexidade dos sistemas de redes móveis. O objetivo concreto é o desenvolvimento de um simulador de forma de onda de Multiplexação por Divisão de Frequência Ortogonal (OFDM) que atinja as taxas efetivas de dados para a 5^a Geração de Comunicações Móveis (5G) utilizando Modulação de Amplitude em Quadratura (QAM), realizar simulações para averiguar o normal funcionamento de acordo com a teoria e realizar testes laboratoriais. Neste estudo é efetuada a estimação de canal, são avaliadas as performances da Taxa de Erro de Bits (BER) e da Magnitude do Vetor de Erro (EVM) como métricas de estudo e efetuado um paralelismo com os modelos de perdas de transmissão usuais para comunicações indoor e de espaço livre. O estudo e os testes laboratoriais concluem-se em comunicações OFDM não codificado e com decisão abrupta em códigos convolucionais efetuadas até velocidades efetivas de 5.9 Gbps de dados e foram obtidos os resultados e medições num ambiente de laboratório, com uma portadora de 3.5 GHz, com o ganho de ambas as antenas de 2dB e um amplificador com um ganho de 26dB em distâncias até aos 4 metros entre as duas antenas. O melhor resultado obtido em termos de velocidade de transmissão de dados foi a comunicação 256-QAM OFDM não codificado atingindo os 5.9 Gbps com 4 metros de distância entre antenas.

Palavras-chave: 5G; OFDM; QAM; Códigos Convolucionais; Estimação de Canal

Abstract

With the years passing by, the users of mobile networks present higher needs and demands when it comes to effective download and upload data rates. The fifth generation of mobile communications assumes the concretization of binary rates above 1 Gbps to be achieved by any ordinary user. To fulfil this requirement, it was necessary to undertake a study and development of a system using the 4th Generation of Mobile Communications (4G) waveform to lessen the need for adding new modules and increasing the complexity of mobile network systems. The main goal is to develop an Orthogonal Frequency Division Multiplexing (OFDM) waveform simulator for 5th Generation of Mobile Communications (5G) using Quadrature Amplitude Modulation (QAM), simulate its performance to compare with the theoretical one and perform laboratorial tests. In this study the channel estimation is carried out and we evaluated the performance of Bit Error Rate (BER) and Error Vector Magnitude (EVM) as study metrics and parallels the usual transmission loss models for indoor and free-space communications. The study and experiments end in resulting mobile uncoded and convolutional hard decision OFDM communications up to 5.9 Gbps of effective data rate and the results and measurements were obtained inside the laboratory environment, with a signal carrier of 3.5GHz and 2dB of both antennas gain and 26dB of amplifier gain at distances up to 4 meters between the two antennas. The best result obtained considering the highest data rate achieved was a 256-QAM uncoded OFDM communication at 5.9 Gbps on a 4 meters distance between antennas.

Keywords: 5G; OFDM; QAM; Convolutional Codes; Channel Estimation

Acknowledgements

I would first like to thank Prof. Francisco Cercas and Prof. Adolfo Cartaxo for the opportunity to develop this project and the availability to supervise this work. I would also thank Prof. Pedro Sebastião, Prof. Nuno Souto, Dr Tiago Alves and Prof. Américo Correia for being available to answer my questions and clear my doubts as well as pointing me in the right direction.

To Instituto de Telecomunicações, Instituto Superior Técnico and ISCTE - Instituto Universitário de Lisboa, thank you for providing the means to enable me to carry out my work.

To my mother and father for making all of this possible, thank you for being there all the time, for your support and for encouraging me to pursue my dreams and to work hard on my personal and professional goals.

A special thanks to all my family, friends and my girlfriend Ana Rita for being at my side throughout my life and especially these last five years where moments of happiness and sadness were naturally present but less because you were all cheering for me. Thank you Diogo Mosteias, Jorge Silva and Gonçalo Bustorff for being my best friends and for being there for me on any occasion.

Last but not the least, I want to thank my friends and colleagues with whom I shared most of the moments of joy and difficulties during my graduation in ISCTE-IUL, thank you Rui Passinhas, João Oliveira, André Almeida, Rúben Dias, Rui Dias and Jorge Santos.

To each and every one of you – Thank you.

Table of Contents

Resumo	v
Abstract	vii
Acknowledgements	ix
Table of Contents	xi
List of Figures	xv
List of Tables	xvii
List of Acronyms	xix
List of Symbols	xxiii
1 Introduction	1
1.1 Motivation and State of the Art	1
1.2 Goals and Research Questions	6
1.3 Outline	6
1.4 Original Contributions	7
2 General Concepts	9
2.1 Mobile Communications and 5G Requirements	9
2.2 Quadrature Amplitude Modulation	13
2.3 Orthogonal Frequency Division Multiplexing	14
2.4 Multipath Fading Channel	18
2.5 Channel Estimation	19
2.6 Path Loss Models	21
2.6.1 Free-Path Model	21
2.6.2 Two-Ray Ground-Reflection Model	22
2.6.3 Six-Rays Model	23
3 Simulation System Set-up	25
3.1 System Control	26
3.2 Transmitter	28
3.2.1 Generate Data Bits Sequence	29
3.2.2 Encoding	29
3.2.3 Interleaving	29

3.2.4	M-QAM Constellation Mapping	29
3.2.5	Normalize QAM Mapped Signal	30
3.2.6	Add Pilot Carriers	30
3.2.7	Serial to Parallel Conversion	32
3.2.8	Insertion of Oversampling Null-Carriers	32
3.2.9	Inverse Discrete Fourier Transform	32
3.2.10	Insertion of Cyclic Prefix	32
3.2.11	Digital to Analog Conversion	33
3.2.12	Parallel to Serial Conversion	33
3.2.13	Low Pass Filter	33
3.2.14	Upconverting to Signal Carrier	34
3.3	Wireless Channel	35
3.4	Additive White Gaussian Noise	36
3.5	Receiver	38
3.5.1	Downconverting to Signal Carrier	38
3.5.2	Low Pass Filter	39
3.5.3	Serial to Parallel Conversion	39
3.5.4	Analog to Digital Conversion	39
3.5.5	Removal of Cyclic Prefix	39
3.5.6	Discrete Fourier Transform	40
3.5.7	Removal of Oversampling Null-Carriers	40
3.5.8	Channel Estimation	40
3.5.9	Parallel to Serial Conversion	41
3.5.10	Equalization	41
4	Experimental Set-up	43
4.1	Hardware Specifications	44
4.1.1	AWG	44
4.1.2	Amplifier	45
4.1.3	Antennas	45
4.1.4	DSO	46
4.2	Set-ups Overview	47
4.3	Offline Synchronism	49
5	Results	51
5.1	Simulation Performance	51
5.1.1	AWGN Channel Performance	52
5.1.2	Rayleigh Channel Performance	55
5.2	Experimental Performance	62
5.2.1	AWG Effective Frequency in Back-to-Back	64
5.2.2	Non-Amplified Wireless	66
5.2.2.1	Antennas Effective Frequency	66
5.2.2.2	Performance along Distance	67
5.2.3	Amplified Wireless	72
5.2.3.1	Performance over Time	72
5.2.3.2	Performance along Distance	73

6	Conclusions and Future Work	77
6.1	Conclusions	77
6.2	Future Work	78
	 Bibliography	 79

List of Figures

2.1	Discrete-time QAM OFDM modulation system model.	17
2.2	Discrete-time QAM OFDM demodulation system model.	17
2.3	Signal structure for a PSAM radio system in time domain.	19
2.4	Signal structure for a PSAM radio system in frequency domain.	20
2.5	Transmission over pilot embedding system.	21
2.6	Two-ray ground reflection model scheme	22
2.7	Six-rays model scheme	23
3.1	General system design for the OFDM simulator	25
3.2	OFDM modulator high-level block diagram.	28
3.3	Encoding and Decoding Trellis of LTE systems.	29
3.4	Pilot distribution scheme over time and frequency	31
3.5	Example of CP insertion with $N_{COFDM} = 16$ and $N_{cp} = 3$	33
3.6	Example of LPF effect in signal during OFDM modulation	34
3.7	OFDM demodulator high-level block diagram.	38
3.8	Example of LPF effect in signal during OFDM demodulation with SNR=15dB and over Rayleigh fading channel	39
4.1	IT laboratory set-up scheme	43
4.2	AWG transmitting an OFDM signal recorded with 1742300 samples	44
4.3	ZVA-183-S+ Amplifier used in wireless experimental set-up	45
4.4	Antenna used in wireless experimental set-up	45
4.5	DSO receiving an OFDM signal recorded with 1742300 samples	46
4.6	Back-to-Back system diagram	47
4.7	Simplified antennas system diagram	48
4.8	Amplified antennas system diagram	49
5.1	64-QAM simulation performance over AWGN channel	53
5.2	64-QAM EVM vs SNR over AWGN channel	53
5.3	256-QAM simulation performance over AWGN channel	54
5.4	256-QAM EVM vs SNR over AWGN channel	54
5.5	Uncoded 64-QAM Mean BER with ZF equalizer over Rayleigh fading channel	55
5.6	Uncoded 64-QAM Mean BER with MMSE equalizer over Rayleigh fading channel	56
5.7	Hard Decision 64-QAM Mean BER with ZF equalizer over Rayleigh fading channel	56
5.8	Hard Decision 64-QAM Mean BER with MMSE equalizer over Rayleigh fading channel	57

5.9	Uncoded 256-QAM Mean BER with ZF equalizer over Rayleigh fading channel	58
5.10	Uncoded 256-QAM Mean BER with MMSE equalizer over Rayleigh fading channel	58
5.11	Hard Decision 256-QAM Mean BER with ZF equalizer over Rayleigh fading channel	59
5.12	Hard Decision 256-QAM Mean BER with MMSE equalizer over Rayleigh fading channel	59
5.13	64-QAM simulation performance over Rayleigh fading channel	60
5.14	64-QAM EVM vs SNR over Rayleigh fading channel	61
5.15	256-QAM simulation performance over Rayleigh fading channel	61
5.16	256-QAM EVM vs SNR over Rayleigh fading channel	62
5.17	Test Bed AWG EVM performance comparison between 4/16/64/256 QAM on 0.6/1.5/2.5/3.5 GHz of carrier frequency	65
5.18	Test Bed AWG BER performance comparison between 4/16/64/256 QAM on 0.6/1.5/2.5/3.5 GHz of carrier frequency	65
5.19	Test Bed antennas measured 4-QAM EVM over carrier frequency	67
5.20	Uncoded 64/256 QAM EVM Performance along distance without amplification	68
5.21	Uncoded 64/256 QAM BER Performance along distance without amplification	68
5.22	System path loss along distance without amplification	71
5.23	Variation of 64-QAM Uncoded BER over 20 realisations at 11cm distance	72
5.24	Variation of 256-QAM Hard Decision BER over 20 realisations at 400cm distance	72
5.25	Uncoded 64/256 QAM EVM Performance along distance with amplification	73
5.26	Uncoded 64/256 QAM BER Performance along distance with amplification	74
5.27	System path loss along distance with amplification	76

List of Tables

1.1	Required EVM values to consider as a valid communication for 5G for each modulation scheme	2
2.1	Comparison of Mobile Generation: 1G To 5G.	10
2.2	Excess tap delay versus relative power model for EPA	18
2.3	Excess tap delay versus relative power model for EVA	18
2.4	Excess tap delay versus relative power model for ETU	19
5.1	OFDM Simulation Signal Parameters	51
5.2	Simulation number of bits and minimum achievable BER in each simulation	52
5.3	OFDM Experimental signal Parameters	63
5.4	Experimental number of bits and achievable BER	63
5.5	Effective data rates for each considered scenario	63
5.6	Test Bed AWG constellations comparison between 4/16/64/256 QAM on 0.6/1.5/2.5/3.5 GHz of carrier frequency	64
5.7	Test Bed antennas received 4-QAM constellations comparison between 0.6/1.5/2.5/3.0/3.5/4.0/5.0 GHz of carrier frequency	66
5.8	BER Comparison between modulation and encoding scenarios for 1.5cm .	69
5.9	BER Comparison between modulation and encoding scenarios for 12.5cm	69
5.10	BER Comparison between modulation and encoding scenarios for 23.5cm	69
5.11	BER Comparison between modulation and encoding scenarios for 34.5cm	69

5.12	BER Comparison between modulation and encoding scenarios for 45.5cm	70
5.13	BER Comparison between modulation and encoding scenarios for 11cm	74
5.14	BER Comparison between modulation and encoding scenarios for 100cm	75
5.15	BER Comparison between modulation and encoding scenarios for 200cm	75
5.16	BER Comparison between modulation and encoding scenarios for 300cm	75
5.17	BER Comparison between modulation and encoding scenarios for 400cm	75

List of Acronyms

1G	1 st Generation of Mobile Communications
3GPP	3 rd Generation Partnership Project
4G	4 th Generation of Mobile Communications
5G	5 th Generation of Mobile Communications
ADC	Analog-to-Digital Converter
ADSL	Asymmetric Digital Subscriber Line
AWGN	Additive White Gaussian Noise
AWG	Arbitrary Waveform Generator
BER	Bit Error Rate
CDF	Cumulative Distribution Function
CFO	Carrier Frequency Offset
CP	Cyclic Prefix
CP-OFDM	Cyclic Prefixed OFDM
DAB	Digital Audio Broadcast
DAC	Digital-to-Analog Converter
DFT	Discrete Fourier Transform
DFT-OFDM	Discrete Fourier Transform OFDM
DL	Downlink
DRB	Digital Radio Broadcast
DSO	Digital Storage Oscilloscope

DVB	Digital Video Broadcast
eMBB	Enhanced Mobile Broadband
EPA	Extended Pedestrian A model
ETU	Extended Typical Urban model
EVA	Extended Vehicular A model
EVM	Error Vector Magnitude
FBMC	Filter Bank Multicarrier
FBMC/OQAM	Quadrature Amplitude Modulation-Based FBMC
FEC	Forward Error Correction
FFT	Fast Fourier Transform
F-OFDM	Filtered OFDM
GFDM	Generalized Frequency Division Multiplexing
ICI	Intercarrier Interference
IDFT	Inverse Discrete Fourier Transform
IFFT	Inverse Fast Fourier Transform
ISI	Intersymbol Interference
IT	Instituto de Telecomunicações
ITU-R	International Telecommunication Union Radio Sector
LDPC	Low-density Parity-Check Codes
LTE	Long Term Evolution
LTE-A	Long Term Evolution Advanced
LoS	Line of Sight
LPF	Low-Pass Filter
MCM	Multicarrier Modulations
mMTC	Massive Machine-Type Communications
OFDM	Orthogonal Frequency Division Multiplexing

OOB	Out-Of-Band power
P2P	Peer-to-Peer
PAPR	Peak-to-Average Power Ratio
PDU	Protocol Data Unit
P-OFDM	Polar-OFDM
PSAM	Pilot Symbol Assisted Modulation
PSD	Power Spectral Density
PSK	Phase-Shift Keying
QAM	Quadrature Amplitude Modulation
QoS	Quality of Service
RF	Radio Frame
SNMC	Slepian basis based Non-orthogonal Multi-Carrier
SNR	Signal-to-Noise Ratio
SRIT	Set of Radio Interface Technologies
TCH	Tomlinson Cercas Hughes Codes
UFMC	Universal Filtered Multicarrier
UF-OFDM	Universal Filtered OFDM
UL	Uplink
UWB	Ultra Wideband
URLLC	Ultra-Reliable Low Latency Communication
WGN	White Gaussian Noise
W-OFDM	Weighted OFDM

List of Symbols

$c_{cp}(kt)$	OFDM signal after CP insertion
C_x	carrier in index x
c_x	chip in index x
$C_{zp}(kf)$	OFDM signal after null-carriers insertion in frequency domain
$c_{zp}(kt)$	OFDM signal after IFFT
d_f	sampling frequency resolution
d_t	sampling time resolution
e_b	linear bit energy in Watts second (Joules) (Ws or J)
E_b	logarithmic bit energy in Watts per Hz (Joules) (W/Hz or J)
E_{est}	equalizer estimated transfer function
e_s	linear symbol energy in Watts second (Joules) (Ws or J)
E_s	logarithmic symbol energy in Watts per Hz (Joules) (W/Hz or J)
f_0	OFDM carriers spacing
f_p	signal carrier frequency
f_s	sampling frequency
g_{plt}	number of carriers in between pilots
$H_{est}(f)$	channel estimated transfer function
$H_f(f)$	Rayleigh fading channel transfer function
i_{plt}	pilots indexes values sequence
$I(t)$	baseband in-phase (real) components of modulated OFDM signal
k_{fpdf}	auxiliar value rate for sampling OFDM signal
$H_{LPF}(f)$	low-pass filter transfer funtion
M	modulation constellation order
N_{cOFDM}	number of OFDM signal carriers
N_{c_p}	number of chips in cyclic prefix
N_{c_T}	total number of chips in OFDM symbol
N_{sOFDM}	number of samples per OFDM symbol
N_{sc}	number of samples per chip
N_{st}	total number of samples in the OFDM signal

N_b	number of data bits
$N_{cff}(t)$	values sequence of AWGN time gaussian coefficients
N_{OFDM}	number of OFDM symbols
N_{plt}	total number of pilot symbols
$N_{sig}(t)$	noise signal
N_{taps}	number of taps of Rayleigh fading channel
n_o	linear noise variance Watts second (Joules) per sample (Ws or J)
N_o	noise variance in Watts per Hz (Joules) per sample (W/Hz or J)
p_{plt}	OFDM signal percentage of pilot symbols
P_n	relative power (in dB) for the n-th channel tap
p_n	linear relative power for the n-th channel tap
p_N	noise power in Watts (W)
N_{PSD}	noise power spectral density
$Q(t)$	baseband quadrature (imaginary) components of modulated OFDM signal
$S_I(t)$	passband in-phase (real) components of modulated OFDM signal
$S_Q(t)$	passband quadrature (imaginary) components of modulated OFDM signal
S_{amps}	interpolated pilots amplitudes sequence
S_{phas}	interpolated pilots phases sequence
SNR	signal to noise ratio in dB
snr	linear signal to noise ratio
$S_{tx}(t)$	transmitted OFDM modulated signal
T_0	OFDM symbol data duration
t_c	chip duration
T_{OFDM}	total OFDM symbol duration (OFDM signal period)
T_P	OFDM symbol cyclic prefix duration
T_W	simulation time window
v_{freq}	simulation frequency vector
v_{time}	simulation time vector
$X_{AWGN}(t)$	OFDM signal after AWGN channel
x_{DAC}	sampled OFDM signal (after DAC)
X_{LPF}	OFDM signal after LPF
$X_{norm}(F)$	normalized OFDM signal in frequency domain
$x_{norm}(t)$	OFDM signal in time domain
$X(F)$	OFDM signal in frequency domain
$x(t)$	OFDM signal in time domain
$Y(f)$	resulting signal in frequency domain after Rayleigh fading channel
$y(t)$	resulting signal in time domain after Rayleigh fading channel

τ_n | delay values sequence for each channel tap

Chapter 1

Introduction

Engineers should be able to plan and develop new tools, features, services, systems, methods and techniques to enhance or even replace the old ones. With the increasing demand for new users, it is important to use good management strategies for the available resources. The rising number of mobile devices that require high data rates is placing increasing demands on bandwidth which requires spectrally efficient radio modulations and resilience against the multipath wireless channel effects.

1.1 Motivation and State of the Art

5G technologies are being developed to meet some parameters that International Telecommunication Union Radio Sector (ITU-R) believe that should be considered as key capabilities of IMT-2020 [1]. Among all the parameters described in [1], it is indicated that peak data rate should be, at least, 20 Gbps Downlink (DL) and 10 Gbps Uplink (UL) where every user must experience around 100 Mbps DL and 50 Mbps UL. Those values of data rate require stronger hardware and more power consumption, and although people are used to getting those rates at home with Wi-Fi technologies and even higher rates in Ethernet over optical fibre, this is not currently a reality when it comes to average radio communication rates. When it comes to planning a radio communication there are several data modulations to consider, usually Phase-Shift Keying (PSK) and QAM. The choice to use QAM over PSK in this work is justified because despite being more complicated, QAM has many advantages in its performance [2]: better noise resistance,

is more adaptive for channel changes but more importantly, QAM has more distance between symbols than PSK when we consider higher modulation orders which translates to a better performance.

The basis for the new proposals is still being developed by the general specifications that Keysight Technologies assume to be the goals and first impressions of what 5G should be at [3], which is based on the 3rd Generation Partnership Project (3GPP) NR release.

Among all the specifications in [3], the white paper concludes that we should consider carrier frequencies in two different frequency ranges: from 410 MHz to 7.125 GHz (as they refer as FR1) and from 24.25 GHz to 52.6 GHz (as RF2). Also, the signal bandwidth should be considered to be up to 100 MHz in FR1 and 400 MHz in FR2. The subcarrier spacing for OFDM should also depend on the carrier frequency range, being 15 kHz, 30 kHz or 60 kHz for FR1 and 60 kHz, 120 kHz or 240 kHz for FR2 carriers. The maximum number of subcarriers is pointed out as 3300 useful subcarriers by an FFT size of 4096 subcarriers. The waveforms that are considered are Cyclic Prefixed OFDM (CP-OFDM) for UL and DL, with QPSK, 16-QAM, 64-QAM and 256-QAM, while Discrete Fourier Transform OFDM (DFT-OFDM) is only considered for UL with $\pi/2$ -BPSK, 16-QAM, 64-QAM and 256-QAM. Sub-6 GHz bands should consider carrier frequencies from 3.4 to 3.7 GHz and from 4.4 to 4.9 GHz due to the complexity of the numerous test cases as explained in [3]. They will also be more of an evolution of the existing Long Term Evolution Advanced (LTE-A) capabilities, and bigger challenges are in the mmWave implementations which we will not consider due bandwidth needed for high bit-rates. Table 1.1 resumes the EVM required for each modulation which are described in [3].

TABLE 1.1: Required EVM values to consider as a valid communication for 5G for each modulation scheme

Modulation	EVM [%]	EVM [dB]
QPSK	17.5	-15.14
16-QAM	12.5	-18.06
64-QAM	8.0	-22.94
256-QAM	3.5	-29.12

These are the first impressions of the community lineups of 5G technologies. The

community has been testing and proposing new waveforms for 5G to improve spectral efficiency and BER performance when compared to OFDM. Those are Generalized Frequency Division Multiplexing (GFDM), Filter Bank Multicarrier (FBMC), Quadrature Amplitude Modulation-Based FBMC (FBMC/OQAM), Universal Filtered Multicarrier (UFMC), Slepian basis based Non-orthogonal Multi-Carrier (SNMC) and some variations of CP-OFDM and DFT-OFDM as Filtered OFDM (F-OFDM), Weighted OFDM (W-OFDM), Polar-OFDM (P-OFDM) and Universal Filtered OFDM (UF-OFDM). The approach of the related work described below, will be concentrated on studying the used frequencies, subcarriers numbers, signal bandwidths and the waveform different proposals that will support our work specifications.

In [4], James, Benjamin and John make a comparison of the performance of OFDM versus GFDM. They have decided to carry out the tests using a carrier of 3.5 GHz, with 128 subcarriers, a CP length of 32 (25%) and the signal bandwidth is 1MHz. Even though they concluded that GFDM is slightly better than OFDM when it comes to end-to-end latency, they have similar performance when it comes to BER and GFDM needs an extra module [4].

In [5], Stagio, Torino and Mondin perform a simulation of multi-rate 5G downlink for CP-OFDM, F-OFDM and W-OFDM in a realistic scenario. They used 1024 subcarriers, modulated with QPSK and 256-QAM over 3 different sub-bands originating a signal aggregated bandwidth of 20 MHz. They conclude that W-OFDM offers better performance with low modulation order while F-OFDM outperforms both W-OFDM and CP-OFDM with high modulation orders [5].

In [6], An, Kim and Ryu they suggest W-OFDM as a new waveform for 5G that aims to improve the spectrum efficiency of 5G mobile communications and compare the nonlinear system performance with OFDM, UFMC [7], FBMC, W-OFDM. They decided to use 64 subcarriers over a 5 MHz signal bandwidth. They conclude that even though the Out-Of-Band power (OOB) performance is better in FBMC, W-OFDM should be considered to 5G since it has low-complexity and simple structure when compared to FBMC [6].

In [8], Balint and Budura assess five waveform candidates capable to handle the carrier frequencies in typical 5G scenarios evaluating the overall downlink and uplink

throughput per user. The candidates studied in [8] are CP-OFDM, W-OFDM, FBMC/OQAM, UFMC and F-OFDM. They do this using QAM modulation over two aggregated carriers: one using 104 subcarriers with 15 kHz of subcarrier spacing and the second one using 26 subcarriers with 60 kHz of subcarriers spacing both generating a signal bandwidth of 3.12 MHz (1.56 MHz each). The simulations show the possibility of mixing different numerologies and waveforms, which can make systems more complex when compared to a simple CP-OFDM system. And they assume that is hard to conclude which of the waveforms meets the requirements of all possible scenarios for 5G and further tests should be made to evaluate Peak-to-Average Power Ratio (PAPR) and the complexity of each signal modulation.

In [9], Yang, Wang and Zhang propose a waveform candidate for 5G called SNMC based on Slepian Basis. They present the transmitter and receiver designs, as the algorithms to perform the modulation and demodulation. The study results in some comparison tests between SNMC and OFDM where they evaluate the BER performance. They carried out these tests using a carrier frequency of 2.5 GHz, with 100 kHz of carrier spacing which generates a signal with 5 MHz of bandwidth. In [9] simulations, they show that SNMC has better BER performance than OFDM when they have the same time-frequency efficiency and experience the same Carrier Frequency Offset (CFO). Although, SNMC modulation needs more modules than OFDM and happens to be a more complex procedure.

In [10], Hazareena and Mustafa present a survey where they generally describe all the strong 5G waveform current candidates as FBMC, GFDM, UFMC and F-OFDM. They compare the structures complexity, time and frequency orthogonality, latency, OOB efficiency and CFO robustness. Overall, they point GFDM has one of the best contenders for 5G [10] but they also refer that F-OFDM is less complex and is compatible with the existing systems.

In [11], Wang, Zaidi, Chen, Luo and Dieudonne evaluate the performance of many 5G waveform candidates such as CP-OFDM, W-OFDM, DFTS-OFDM, UF-OFDM and FBMC/OQAM, considering hardware impairments. The carrier frequencies they consider are 6 GHz, 28 GHz and 82 GHz, an FFT size of 4096 over 16-QAM, 7% of Cyclic Prefix (CP) length and different carrier spacings as 20 kHz, 60 kHz and 480 kHz depending on the signal carrier. They test the performance of these scenarios over Additive

White Gaussian Noise (AWGN) channel with a bandwidth of 102 MHz, 204 MHz and 1.632 GHz. This is the closest approach to ours, considering the greatest bandwidth, and CP size equal to the labelled value for 4G communications, but since they are using 16-QAM, the effective data rates are still smaller than the ones we meant to acquire in our transceiver. Among all those waveform candidates, they conclude that for mm-wave communication considering phase noise and non-linear models, all the waveforms have similar performances in terms of EVM and BER and no waveform performing better than CP-OFDM [11] as one more indicator that CP-OFDM is the modulation we should really consider to use.

In [12] and [13], Weitkemper, Koppenborg, Bazzi, Rheinschmitt, Kusume, Samardzija, Fuchs, Benjebbour and Kishiyama also perform a study and experiments to compare CP-OFDM, FBMC/OQAM and UF-OFDM. They use 2.6 GHz as the carrier frequency, 15 kHz as subcarrier spacing, an FFT size of 1024 over QPSK and 16-QAM. The signal has a bandwidth of 9MHz and its performance is evaluated over AWGN and Extended Vehicular A model (EVA) multipath fading channels. Once more, the conclusion is that even though the other techniques have a slightly better performance, the difference to CP-OFDM performance is not enough to consider changing the modulation already used in 4G DL since the other techniques usually need more modules in the terminals.

Overall, CP-OFDM is still a better option to use in 5G communications. In spite of what has been said in [3], the community seems to be more focused on building new waveform proposals than improving the current LTE-A models to achieve the 5G requirements. So our motivation is to keep the complexity of 4G current modules and just focus on improving the effective data rate of the communication, since 4G generally achieves 1Gbps and 5G aims to reach the 10/20Gbps . So the transceiver will be a CP-OFDM transceiver, below 6 GHz as signal carrier, which leads to subcarriers spacings below 60 kHz and a signal bandwidth of 1GHz that is close to the 800 MHz proposed by [3]. To achieve high data rates, a signal bandwidth of 1 GHz and respecting the below 60 kHz subcarrier spacing, our system needs 16384 subcarriers. The main motivation is to understand how all these techniques can be combined and conceive a high-rate transceiver that can be used in 5G communications but maintaining the complexity of the current 4G networks and terminals using CP-OFDM modulation.

1.2 Goals and Research Questions

The main objective of this thesis is to develop a transceiver using the techniques referred in Section 1.1, performing channel estimation using common radio communications techniques, focusing on communication rate as high as possible (always considering the parameters preestablished by ITU-R). For this reason, a MATLAB R2018b program is needed to generate different kinds of radio signals, with different characteristics, different frequencies and bandwidth and evaluate their behaviour and response in time and frequency domains.

Concretely and briefly, the objectives of this dissertation are:

1. Study of high-speed radio communications systems.
2. Carry out channel estimation with several types of sequences.
3. Simulation and implementation of the studied system and its sub-systems.

According to the goals mentioned above and the techniques that will shape the communication, is it possible to design a radio OFDM transceiver for predicted 10Gbps and 20Gbps 5G link rates? Which are the system constraints that QAM and OFDM will impose? Thinking about the characteristics of the transceiver as a whole, can this be useful in future research and the marketplace? These are the main questions that this work aims to answer.

1.3 Outline

The thesis is comprised of 6 chapters.

In chapter 2, the general concepts of mobile communications are described such as an analysis of the history of mobile communications. The transceiver techniques are analysed and discussed.

In chapter 3, the simulation set-up is described. The elements of the transceiver are explained such as the implementation.

In chapter 4, the experimental set-up is described. The hardware main specifications and limitations are also assessed, including the Arbitrary Waveform Generator (AWG), the amplifier, the antennas and the Digital Storage Oscilloscope (DSO).

In chapter 5, the simulation and experimental limitations are assessed. The results of simulation and experiments are presented, analysed and discussed.

In chapter 6, the conclusions are discriminated and future work line-ups are described.

1.4 Original Contributions

In the author's opinion, the main contributions of this thesis are the following:

- Simulation and experimental results of a radio OFDM communication with 1 GHz bandwidth at 3.5 GHz of carrier frequency
- Performance of a SISO OFDM radio connection with 1.5 Gbps, 2.0 Gbps, 4.4 Gbps, 5.9 Gbps of effective bit-rate up to 4m which can be used for indoor communications or micro cellular systems
- Performance and proposal of an adapted CP-OFDM 5G waveform based on 4G specifications
- "5.9 Gbps Test Bed OFDM for 5G" article submitted in the 13th Congress of the Portuguese Committee of URSI (ANACOM-URSI)

Chapter 2

General Concepts

The study and implementation of radio communication involve a considerable set of concepts that should be consolidated to understand how it works and how it should perform according to its characteristics. This chapter is aimed at giving an overview to the general concepts of the communication such as a historical brief of mobile communications until 5G, how do QAM and OFDM work, the considered multipath channel mode, what is channel estimation and how it can be performed and concluding with the path loss models considered to be possible in the experimental environment.

2.1 Mobile Communications and 5G Requirements

In the last few decades, mobile communications networks and devices have experienced a remarkable change. Each generation up to The 4G have some standards, and they consist of different capacities, new techniques and new features that changed the system and its nature.

The 5G will focus on three must-have service categories: Ultra-Reliable Low Latency Communication (URLLC), Enhanced Mobile Broadband (eMBB) and Massive Machine-Type Communications (mMTC).

URLLC, as itself indicates an ultra-reliable low latency communication, must support high reliability and low latency services, especially for latency-sensitive devices like in factory automation, autonomous driving, sensor networks that deal with people's physical safety like aeroplanes autopilot system, remote surgery, among others.

eMBB consists of enhanced mobile broadband, which means that we should be able to use a high bandwidth for internet access, which is translated to a high bit rate of data. This is the access service we already have in 4G for mobile smartphones.

mMTC services require that machines should be able to communicate without a server or entity in the middle, just like a Peer-to-Peer (P2P) link. This is required because the main purpose of 5G is to decentralize data flows to speed up communications and network availability.

To take a close look at the main differences between generations, J. Vora presents Table 2.1 in [14].

TABLE 2.1: Comparison of Mobile Generation: 1G To 5G.

Technology	1G	2G	3G	4G	5G
Start/Deployment	1970-80	1990-2004	2004-10	Now	Soon (probably by 2020)
Data Bandwidth	2 kbps	64 kbps	2 Mbps	1 Gbps	Higher than 1 Gbps
Technology	Analog	Digital	CDMA 2000, UMTS, EDGE	Wi-Max, Wi-Fi, LTE	WWWW
Core Network	PSTN	PSTN	Packet N/W	Internet	Internet
Multiplexing	FDMA	TDMA/CDMA	CDMA	CDMA	CDMA
Switching	Circuit	Circuit, Packet	Packet	All Packet	All Packet
Primary Service	Analog Phone Calls	Digital Phone Calls and Messaging	Phone Calls, Messaging, Data	All-IP Service (including Voice Messages)	High speed, High capacity and provide large broadcasting of data in Gbps
Key differentiator	Mobility	Secure, Mass adoption	Better Internet experience	Faster Broadband Internet, Lower Latency	Better coverage and no dropped calls, Much lower latency, Better performance
Weakness	Poor spectral efficiency, major security issue	Limited data rates, difficult to support demand for internet and e-mail	Real performance fail to match type, failure of WAP for internet access	More battery use, Required complicated and expensive hardware	?

As shown in Table 2.1, since 1st Generation of Mobile Communications (1G) data bandwidth has increased from 2kbps to 1Gbps, and the aim for the next generation will be higher bandwidth, higher speed, higher capacity, better coverage, lower latency and large broadcasting of data in Gbps.

According to the ITU-R in [1], 5G parameters should be:

1. Peak Data Rate: the maximum achievable data rate under ideal conditions, expressed in bits/s. Should be 20 Gbit/s DL and 10 Gbit/s UL for eMBB usage scenario.

2. Peak Spectral Efficiency: the maximum data rate under ideal conditions normalized by channel bandwidth, expressed in bit/s/Hz. Should be 30 bit/s/Hz DL and 15 bit/s/Hz UL for eMBB usage scenario.
3. User Experienced Data Rate: the 5% point of the Cumulative Distribution Function (CDF) of the user throughput, expressed in bit/s. Should be 100 Mbit/s DL and 50 Mbit/s UL for eMBB usage scenario.
4. 5th Percentile of User Spectral Efficiency: the 5% point of the CDF of the normalized user throughput, expressed in bit/s/Hz. In an indoor environment should be 0.3 bit/s/Hz DL and 0.21 bit/s/Hz UL; for a dense urban environment should be 0.225 bit/s/Hz DL and 0.15 bit/s/Hz UL and for rural should be 0.12 bit/s/Hz DL and 0.045 bit/s/Hz UL for eMBB usage scenario.
5. Average Spectral Efficiency: the aggregate throughput of all users, expressed in bit/s/Hz/TRxP. In an indoor environment should be 9 bit/s/Hz/TRxP DL and 6.75 bit/s/Hz/TRxP UL; for a dense urban environment should be 7.8 bit/s/Hz/TRxP DL and 5.4 bit/s/Hz/TRxP UL and for rural should be 3.3 bit/s/Hz/TRxP DL and 1.6 bit/s/Hz/TRxP UL for eMBB usage scenario.
6. Area Traffic Capacity: the total traffic throughput served per geographic area, expressed in Mbit/s/m² and the target value is 10 Mbit/s/m² in the indoor environment for eMBB usage scenario.
7. User Plane Latency: the amount of time that the radio network adds since the source sends the packet to when it is received by its destination, expressed in ms. It should be around 4 ms for eMBB, and 1 ms for URLLC.
8. Control Plane Latency: the transition time from an idle state to the active state (continuous data transfer), expressed in ms. It should be 20 ms for eMBB and URLLC.
9. Connection Density: the number of devices that fulfil a specific Quality of Service (QoS) per unit area, expressed in devices/km². It should be around 1 000 000 devices per km².
10. Energy Efficiency: the capability of a Set of Radio Interface Technologies (SRIT) to minimize the network's consumption concerning the traffic capacity provided. The

SRIT should be able to support high sleep ratio and long sleep duration, focusing on efficient data transmission in a loaded case and low energy consumption when there is no data, all for evaluation in the eMBB usage scenario.

11. Reliability: the success probability of transmitting a layer 2/3 packet within a required maximum time. This requirement is defined for evaluation in the URLLC usage scenario and should be 1×10^5 success probability of transmitting a layer 2 Protocol Data Unit (PDU) of 32 bytes within 1 ms, assuming small application data.
12. Mobility: the maximum mobile station speed at which a defined QoS can be achieved, expressed in km/h. Classes of mobility defined: stationary - 0 km/h; pedestrian - 0km/h to 10 km/h; vehicular - 10 km/h to 120 km/h and high speed vehicular - 120 km/h to 500 km/h. The values for normalized traffic channel link data rate, expressed in bit/s/Hz should be 1.5 bit/s/Hz indoor considering 10 km/h of mobility; 1.12 bit/s/Hz considering 30 km/h and 0.8 to 0.45 bit/s/Hz from 120 - 500 km/h. All these values are defined for eMBB usage scenario.
13. Mobility Interruption Time: the shortest time duration during which a user terminal cannot exchange user plane packets with any base station during transitions, expressed in ms. This is defined for eMBB and URLLC usage scenarios and should be 0 ms.
14. Bandwidth: the maximum aggregated system bandwidth, expressed in Hz and may be supported by single or multiple radio frequency carriers. Bandwidth values should be at least 100 MHz and the SRIT must support values up to 1 GHz for operation in higher carriers (above 6 GHz), and the ability to operate with different bandwidths.

It is clear that 5G will change radio communications, and will certainly make world-wide communications work from wireless links and community is currently working to make all of these requirements possible and make a remarkable change in the world of communications as we know it.

2.2 Quadrature Amplitude Modulation

QAM is a form of modulation used for modulating data signals onto a carrier used for radio communications. The QAM signal consists in two carriers shifted in phase by 90 degrees (one-quarter of a cycle, from which the term quadrature arises) where the resulting output consists in both amplitude and phase variations, as an amplitude and phase modulation.

Considering a M -ary QAM and a sequence of N_b bits, it should start by creating blocks of $\log_2 M$ bits to be translated. If N_b is not a multiple of $\log_2 M$, zeros should be added to the end of the sequence.

Assuming M as a result of an even power of 2, this means that $M = 2^{2n}$, the M -ary QAM constellation can be obtained by creating a signal constellation matrix with the coordinates of the k -th signal constellation point:

$$IQ_k = \begin{bmatrix} (-\sqrt{M} + 1, j(\sqrt{M} - 1)) & (-\sqrt{M} + 3, j(\sqrt{M} - 1)) & \dots & (\sqrt{M} - 1, j(\sqrt{M} - 1)) \\ (-\sqrt{M} + 1, j(\sqrt{M} - 3)) & (-\sqrt{M} + 3, j(\sqrt{M} - 3)) & \dots & (\sqrt{M} - 1, j(\sqrt{M} - 3)) \\ \dots & \dots & \dots & \dots \\ (-\sqrt{M} + 1, j(-\sqrt{M} + 1)) & (-\sqrt{M} + 3, j(-\sqrt{M} + 1)) & \dots & (\sqrt{M} - 1, j(-\sqrt{M} + 1)) \end{bmatrix}$$

Assuming $K = \log_2 M$, every combination of K bits is translated to the specific mapped element $a_k + jb_k$ in the constellation matrix IQ_k , which means that the matrix IQ_k , applied to the sequence of N_b bits, generates a sequence of $\frac{N_b}{K}$ imaginary symbols which is our QAM modulated sequence.

To demodulate the QAM sequence, the idea is to apply the same matrix, and get the binary sequence which was translated to that specific received symbol. That means that the received symbol sequence is evaluated using a decision algorithm to translate the received symbols into the symbols that compose the M -ary QAM constellation IQ_k . By the time when the decision is completed, every $a_k + jb_k$ symbol of the constellation is remapped into a sequence of K bits and the original bit sequence is recovered.

Since QAM modulates amplitude as well as phase, makes itself more spectrally efficient. Although, QAM has some disadvantages in its use. For higher modulation orders,

the close distance between QAM constellation symbols makes it more susceptible to noise interference and the receiver will have to carry it out being more complex when compared to PSK. Finally, as QAM amplitude components represent binary data, linearity should be maintained and that leads to the use of a linear amplifier which raises the system's overall power consumption. In spite of having all those disadvantages, this work has the objective of conceiving a high-rate transceiver and because of that, the spectral efficiency is one of our main concerns and is the main advantage in QAM systems[2].

2.3 Orthogonal Frequency Division Multiplexing

OFDM is a modulation format that is being used for many wireless and telecommunications standards such as wireless local area networks as Wi-Fi IEEE 802.11, wireless metropolitan area networks as WiMAX 802.16e, Asymmetric Digital Subscriber Line (ADSL) ITU G.992.1, cellular telecommunications Long Term Evolution (LTE) and LTE-A, Digital Radio Broadcast (DRB) with Digital Audio Broadcast (DAB) and Digital Video Broadcast (DVB), and many more. This technique belongs to a wider class of Multicarrier Modulations (MCM) in which the data information is carried over many modulated narrowband close-spaced subcarriers. The concept of OFDM was first introduced by Robert W. Chang of Bell Labs in [15] and the term appeared in his patent [16].

A OFDM signal consists of the parallel transmission of several signals modulated at different Δf spaced carriers that must be orthogonal in frequency. The binary sequence, which forms the input of the OFDM modulator is subdivided into groups of K bits used to generate blocks of N symbols, where each symbol modulates a different carrier.

Considering T_0 as the time that is used for transmitting each one of the symbols of the corresponding carrier, orthogonality among different transmissions can be achieved by adopting $\Delta f = 1/T_0$. Also, a guard interval T_G is introduced between the transmission of subsequent blocks and is generally used for transmitting a copy of the final border section of the OFDM symbol, called the CP. It is introduced to maintain receiver carrier synchronization at the receiver in the presence of time-dispersive channels and to allow the cyclic convolution between the OFDM signal and the channel response to model

the transmission system. That said, the guard time is used to prevent Intersymbol Interference (ISI) and Inter-carrier Interference (ICI).

The total OFDM symbol duration is $T_{OFDM} = T_0 + T_G$ leading to a maximum symbol rate R_s given by [17]:

$$R_s = \frac{N}{T_{OFDM}} = \frac{N}{T_0 + T_G} \quad (2.1)$$

where the actual OFDM signal bandwidth BW that can be used for data is:

$$BW = \frac{N}{T_0} \quad (2.2)$$

All modulators use the same rectangular shape $g_T(t)$ of finite duration T_{OFDM} given by [17]:

$$g_T(t) = \begin{cases} \sqrt{\frac{1}{T_{OFDM}}} & \text{for } -T_G = T_0 - T_{OFDM} \leq t \leq T_0 \\ 0 & \text{elsewhere} \end{cases} \quad (2.3)$$

As explained in [17], if $c_m = a_m + jb_m$ represents a generic symbol of the modulation, the OFDM signal $x(t)$ corresponding to a block of N symbols is given by [17]:

$$x(t) = g_T(t) \sum_{m=0}^{N-1} [a_c(m) - b_c(m)] \quad (2.4)$$

with, $a_c(m) = a_m \cos(2\pi(f_p + f_m)t + \phi)$ and $b_c(m) = b_m \sin(2\pi(f_p + f_m)t + \phi)$ while the corresponding complex envelope is defined as [17]:

$$\underline{x}(t) = g_T(t) \sum_{m=0}^{N-1} c_m e^{j2\pi f_m t} \equiv \sum_{m=0}^{N-1} c_m \varphi_m(t) \equiv g_T(t) S(t) \quad (2.5)$$

in which $\varphi_m(t) = g_T(t) e^{j2\pi f_m t}$, and $S(t)$ is a periodic function of period T_0 .

The simplest way of implementing an OFDM modulator was first suggested by Weinstein and Ebert in [18] where they adopt a digital structure by using the Discrete Fourier Transform (DFT). The digital transmission of the OFDM signal in Equation 2.4 corresponds to the transmission of a sampled version of the complex envelope in Equation 2.5, that is, the transmission of the following sequence [17]:

$$\underline{x}[n] = \underline{x}(nt_c) = g_T(nt_c) \sum_{m=0}^{N-1} c_m e^{j2\pi f_m t_c} \quad (2.6)$$

where t_c is the sampling period. Following the Equation 2.4, we understand that $x(t)$ consists of a parallel transmission of N signals which occupy $2\Delta f$, and modulate carriers spaced by Δf . Because of that, it is correct to assume that the complex envelope in Equation 2.5 will require a range of frequencies $[-B, B]$, where $B = N \times \frac{\Delta f}{2}$. That said, the complex envelope can be represented by samples taken with a period $t_c = \frac{T_0}{N}$ [17]:

$$\underline{x}[n] = g_T(nt_c) \sum_{m=0}^{N-1} c_m e^{\frac{j2\pi f_m n T_0}{N}} \quad (2.7)$$

Futhermore, assuming $f_m = m\Delta f - \frac{N}{2}$ and $\Delta f = \frac{m}{T_0} - \frac{N}{2T_0}$ [17]:

$$\underline{x}[n] = g_T(nt_c) \sum_{m=0}^{N-1} c_m e^{j\frac{2\pi m n}{N}} e^{-j\pi n} = g_T(nt_c) (-1)^n \sum_{m=0}^{N-1} c_m e^{j\frac{2\pi m n}{N}} \quad (2.8)$$

The summation in Equation 2.8 corresponds to the n -th element of vector \underline{C} which represents the Inverse Discrete Fourier Transform (IDFT) of the vector $\{c_0, \dots, c_n, \dots, c_{N-1}\}$, which leads to [17]:

$$\underline{x}[n] = g_T(nt_c) (-1)^n C_n \quad (2.9)$$

The Equation 2.9 indicates that the samples of the complex envelope can be obtained by computing the IDFT of the set os points with coefficients $\{c_0, \dots, c_n, \dots, c_{N-1}\}$. However, Van Nee and Prasad in [19] suggest that the serial transmission of the sequence in Equation 2.9 does not allow the reproduction of a real OFDM signal since the absence of oversampling would introduce intolerable aliasing when passing this sequence in a Digital-to-Analog Converter (DAC). Because of that, they came up with a solution, and it consists of introducing zero padding, before computing the IDFT, in the input sequence $\{c_0, \dots, c_n, \dots, c_{N-1}\}$. Although being a solution, this requires the introduction of additional sub-carriers. The padding zeros should be added in the middle of the input vector because the added sub-carriers will be located at the frequency vector edges and will not interfere with the original OFDM signal sub-carriers [17].

Since the IDFT is a periodic sequence with period N , the introduction of the CP in the digital domain is performed by appending the last $N_G = T_G/t_c$ elements of the original sequence in Equation 2.9 to the beginning of the sequence itself.

Figure 2.1 and 2.2 illustrate the main steps that the OFDM modulator and demodulator should perform.

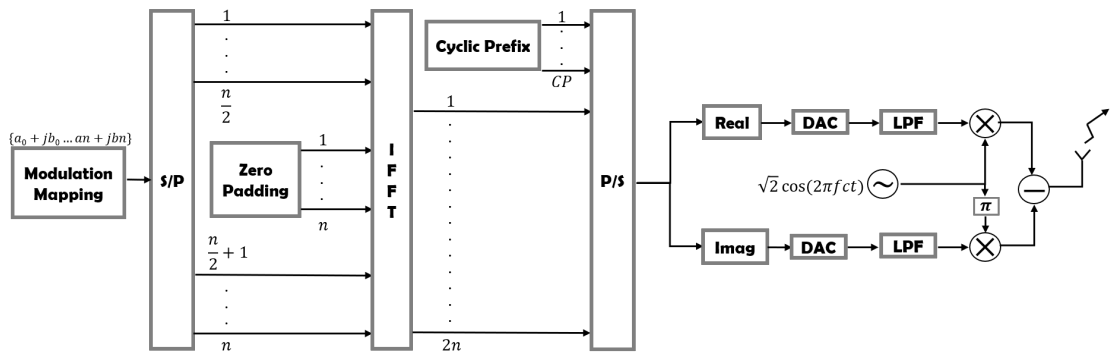


FIGURE 2.1: Discrete-time QAM OFDM modulation system model.

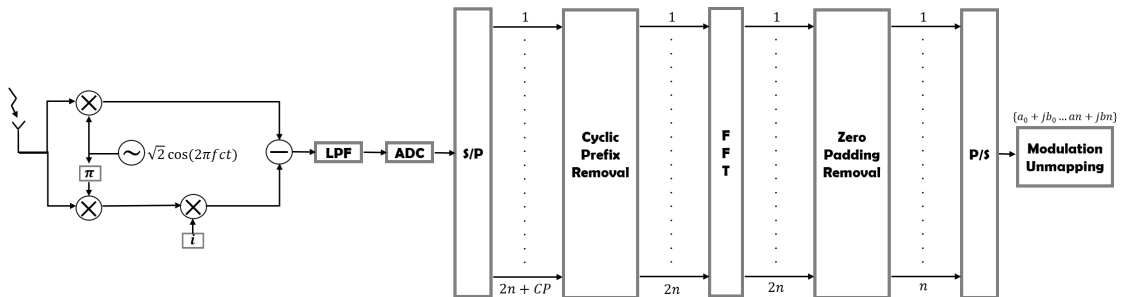


FIGURE 2.2: Discrete-time QAM OFDM demodulation system model.

There are some advantages that a system can obtain by using OFDM, as robustness to dispersion, high spectral efficiency, the capability of a dynamic bit and power loading and the most important is the ease of phase and channel estimation in a time-varying environment. But even though it is the main technique used in radio communications nowadays, the community had difficulty to accept and use OFDM because it generates a high PAPR and has a significant frequency offset and phase noise sensitivity that leads to ICI [20].

2.4 Multipath Fading Channel

In wireless communications, multipath is the phenomenon that is generated when radio signals reach the receiving antenna by two or more paths, generally due to atmospheric ducting, ionospheric reflection and refraction and reflection from water bodies and terrestrial objects. This phenomenon causes multipath constructive and destructive interference summed with some phase shifting, which means that the magnitudes of the many arriving signals by the various paths have a Rayleigh distribution know as Rayleigh fading. Considering mobile radio communications, there are three 3GPP delay profiles to consider: Extended Pedestrian A model (EPA), EVA and Extended Typical Urban model (ETU). These channel models are classified based on low, medium and high delay spread where low delay spreads are used to model indoor environments with small cell sizes while medium and high delay spreads are used to model urban environments with large cells. Their delay profile can be found in Tables 2.2, 2.3 and 2.4, respectively [21].

TABLE 2.2: Excess tap delay versus relative power model for EPA

Excess Tap Delay [ns]	Relative Power [dB]
0	0.0
30	-1.0
70	-2.0
90	-3.0
110	-8.0
190	-17.2
410	-20.8

TABLE 2.3: Excess tap delay versus relative power model for EVA

Excess Tap Delay [ns]	Relative Power [dB]
0	0.0
30	-1.5
150	-1.4
310	-3.6
370	-0.6
710	-9.1
1090	-7.0
1730	-12.0
2510	-16.9

These are the most used delay profiles for mobile communications and allow us to make a good simulation of a real wireless channel environment.

TABLE 2.4: Excess tap delay versus relative power model for ETU

Excess Tap Delay [ns]	Relative Power [dB]
0	-1.0
50	-1.0
120	-1.0
200	0.0
230	0.0
500	0.0
1600	-3.0
2300	-5.0
5000	-7.0

2.5 Channel Estimation

The wireless radio channel can be parameterized as a combination of paths and the signal gets distorted while goes through it. Channel estimation is a process to characterize the channel to properly decode the received signal and remove the distortion applied through its path. Channel estimation has two different implementation methods: Pilot Symbol Assisted Modulation (PSAM) and Pilot Embedding.

PSAM was proposed in [22][23] and consists of pilot symbols periodically inserted into data sequence as explained in [24].

Considering a Radio Frame (RF) as data symbols plus the pilot symbol(s) or plus a training sequence, the signal can be illustrated with three RF in Figure 2.3 which are transmitted sequentially over time.

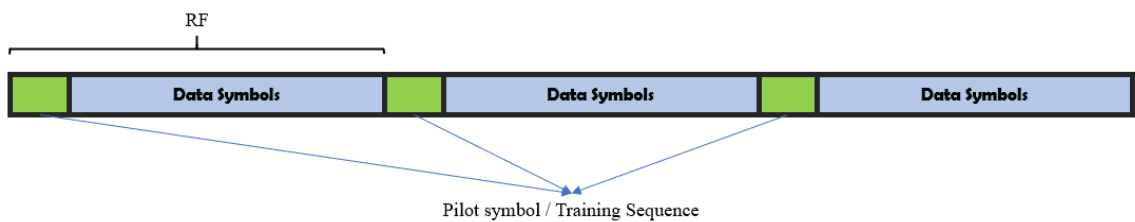


FIGURE 2.3: Signal structure for a PSAM radio system in time domain.

Due to this time multiplexing of pilot and data symbols, some of the available bandwidth must be consumed to accomplish their transmission. This is evident because of the transmission time T_p that pilots occupy, in the time domain, corresponds to a frequency width of Δf in the frequency domain. That means, in the case of OFDM, PSAM can be accomplished by adding more subcarriers to the system, what will keep our effective data

transfer rate, or even use some of the already existing subcarriers as shown in Figure 2.4 that will reduce our effective data transfer rate depending on the number of subcarriers used for channel estimation.

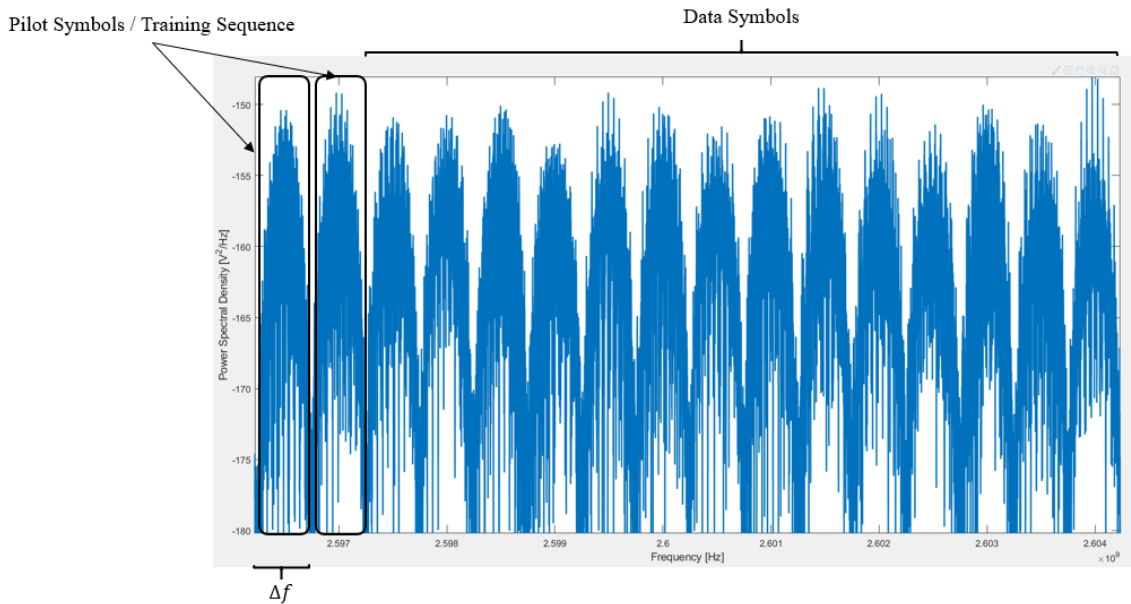


FIGURE 2.4: Signal structure for a PSAM radio system in frequency domain.

The pilot symbols insertion rate must fulfil the Nyquist sampling theorem. So, considering B has the maximum frequency of the input signal and f_s the frequency needed to sample that continuous-time input signal is

$$f_s \geq 2B \quad (2.10)$$

Despite this definition, Nyquist Theorem assumes an infinite number of samples and a noiseless channel, which is undoable in real wireless communications due to path losses and White Gaussian Noise (WGN). Because of that, the actual pilot insertion rate must be higher than just twice the maximum frequency of the input signal. This is beneficial because enables the creation of channel behaviour pattern which consists in mapping each possible transmitted symbol to its received quadrature amplitude shifted symbol. After the transmission and estimation, the obtained sequence of pilot symbol channel estimates must then be interpolated to map a channel estimate for each information symbol.

Pilot Embedding method is proposed in [25]. It still uses pilot symbols, but the pilot symbols or training sequences are summed to the data sequence and transmitted

simultaneously. This means that a pilot channel can be transmitted in parallel with the data channels by reserving a spreading code for it as explained in [24].

Considering a few data physical channels, Figure 2.5 illustrates how the transmission is performed under Pilot Embedding technique.

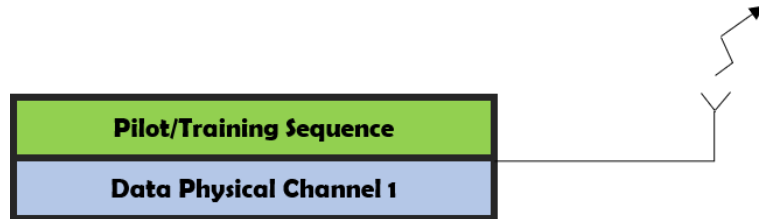


FIGURE 2.5: Transmission over pilot embedding system.

The approach to estimate is close to the one used in [25], when in the case of a flat fading environment, channel coefficients can be estimated by first despreading the pilot channel, multiplying the despreading pilot symbols by its conjugate and then applying a filter to the noisy channel estimates using a moving average filter. Since the data channels have different data rates when compared with the pilot symbol rate, interpolation is needed over the channel estimates to match the rates. This approach requires more power when sending data plus the pilot sequences, but the system preserves the bandwidth available for the communication and consequently, it preserves the effective data transfer rate. The code blocks or sequences that are used as pilots to perform the channel estimation can vary and it is up to the engineer to decide which one has the best performance according to the system requirements. There are many examples like Tomlinson Cercas Hughes Codes (TCH), Zadoff-Chu (Cazac), PN-sequences, m-sequences, orthogonal sequences, complementary sequences, Barker Codes, and many more.

2.6 Path Loss Models

2.6.1 Free-Path Model

The free-space path loss formula derives from the Friis transmission formula [26][27] and is given by

$$\frac{P_r}{P_t}[dB] = Dt + Dr + 20 \log_{10} \left(\frac{\lambda}{4\pi d} \right) \quad (2.11)$$

where P_r is the received signal power, P_t the transmitted signal power, Dt the transmitter antenna directivity, Dr the receiver antenna directivity, λ the wavelength and d as the distance between both antennas.

The fact that our antennas are almost isotropic, the formula above can be simplified and written as:

$$\frac{P_r}{P_t}[dB] = 20 \log_{10} \left(\frac{\lambda}{4\pi d} \right) \quad (2.12)$$

This model is not accurate to our indoor measurements, but we will try to analyse how different it is from our measurements.

2.6.2 Two-Ray Ground-Reflection Model

Figure 2.6 illustrates the concept of the reflections in two-ray ground-reflection model.

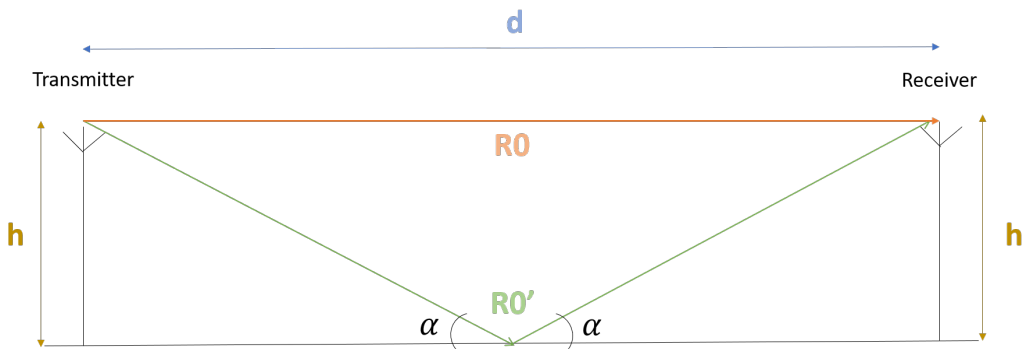


FIGURE 2.6: Two-ray ground reflection model scheme

Considering that the antennas are in the center of the room and at a distance d from each other, both at a height h and with G_t and G_r as the transmitter and receiver antenna gains, R_0 and R_0' define the length of the Line of Sight (LoS) ray and its reflection in the ground and are given by:

$$R_0 = d \quad (2.13)$$

and

$$R'_0 = \sqrt{d^2 + (2h)^2} \quad (2.14)$$

Assuming Γ has the reflection path coefficient (-1 if perfect ground), the resulting channel complex coefficient of the transmission considering both rays is identified in [26][27] as:

$$p_0(t) = \frac{\lambda}{4\pi i} \left(\frac{e^{j \cdot 2\pi \cdot \frac{R_0}{\lambda}}}{R_0} + \Gamma \frac{e^{j \cdot 2\pi \cdot \frac{R'_0}{\lambda}}}{R'_0} \right) \quad (2.15)$$

and the estimated path loss is given by

$$P_l(dB) = 20 \log_{10} |p_0(t)| \quad (2.16)$$

2.6.3 Six-Rays Model

Figure 2.7 illustrates the concept of the wall reflections in six-rays model.

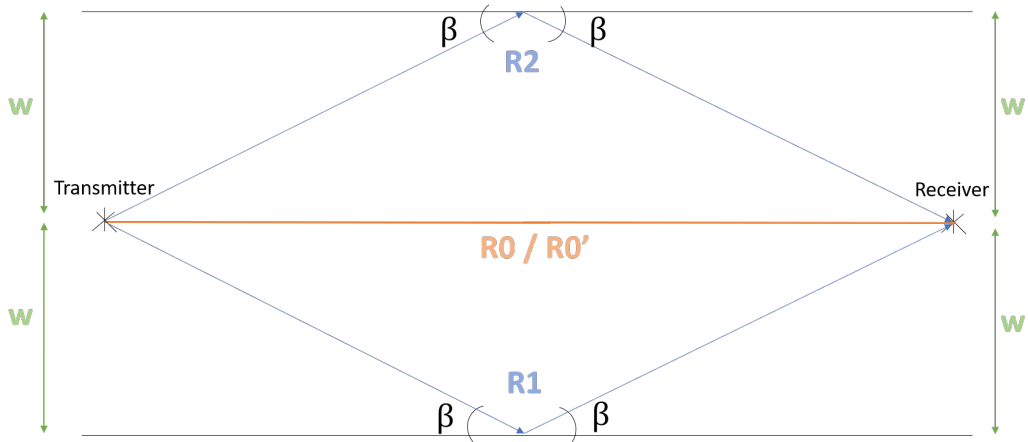


FIGURE 2.7: Six-rays model scheme

The six-rays model is the closest model to compare with our laboratory transmission. This model considers the direct ray and the direct reflection on ground loss as in Equation 2.15 and also adds the wall reflections and the reflections on the ground of each wall reflection. That said, considering w as the perpendicular distance from the antennas to the walls, the resulting lengths of reflection in walls ($R1$ and $R2$) and ground after walls ($R1'$ and $R2'$) and are given by:

$$R_1 = \sqrt{d^2 + (2w)^2} \quad (2.17)$$

$$R'_1 = 2\sqrt{\left(\frac{R_1}{2}\right)^2 + (2h)^2} \quad (2.18)$$

and since they're equally spaced from walls,

$$R_2 = R_1 \quad (2.19)$$

and

$$R'_2 = R'_1 \quad (2.20)$$

The resulting complex coefficients of each ray considered is the same principle of the two-ray model for each wall reflection and is given by [26][27]:

$$p_1(t) = \frac{\lambda}{4pi} \left(\frac{e^{j \cdot 2\pi \cdot \frac{R_1}{\lambda}}}{R_1} + \Gamma \frac{e^{j \cdot 2\pi \cdot \frac{R'_1}{\lambda}}}{R'_1} \right) \quad (2.21)$$

$$p_2(t) = \frac{\lambda}{4pi} \left(\frac{e^{j \cdot 2\pi \cdot \frac{R_2}{\lambda}}}{R_2} + \Gamma \frac{e^{j \cdot 2\pi \cdot \frac{R'_2}{\lambda}}}{R'_2} \right) \quad (2.22)$$

resulting in a path loss given by

$$P_l(dB) = 20 \log_{10} \left| \sum_{i=0}^N P_i \right| \quad (2.23)$$

Chapter 3

Simulation System Set-up

In order to properly simulate the OFDM waveform and its de/modulation, this system works accordingly to the following assumptions:

1. Transmitter and receiver are perfectly synchronized.
2. Since a cyclic prefix is used, the impulse response of the channel is shorter than the cyclic prefix duration.
3. Channel noise is additive, white and complex Gaussian.

That said, this chapter aims to describe the assumptions, methods and techniques used along the development process of the OFDM system simulator, and is divided in simulation control, the transmitter, the channel, the AWGN and the receiver as illustrated in Figure 3.1:

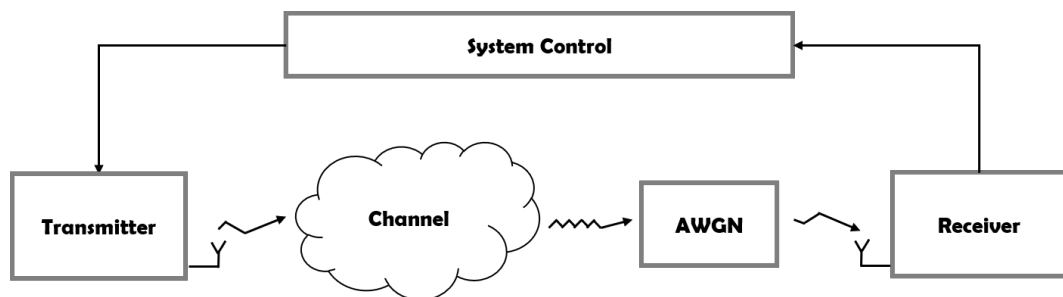


FIGURE 3.1: General system design for the OFDM simulator

3.1 System Control

To control the Rayleigh fading channels, the taps' coefficients are generated in the beginning of the simulation and every simulation can run with a different channel or the same as previous simulations. The whole process of generating a channel model will be explained further in Wireless Channel section.

As a discrete-time OFDM system, the first thing to do is defining the time and frequency vectors. The following steps assume N_{OFDM} as the number of generated OFDM symbols, N_{COFDM} as the number of OFDM chips/subcarriers and M as the QAM modulation index.

The number of CP chips (N_{cp}) is defined by a percentage of the N_{COFDM} which is 6.95% in 4G technologies.

So we achieve a total number of OFDM symbol chips of

$$N_{cT} = N_{COFDM} + N_{cp} \quad (3.1)$$

In order to properly simulate the waveform of the OFDM signal, considering f_s as the sampling frequency, f_0 as the carrier spacing and N_{sc} as the number of samples per chip, we must consider that:

$$\frac{f_s}{f_0} = N_{sc} \times N_{COFDM} \quad (3.2)$$

So, according to the Equation 3.2, $\frac{f_s}{f_0}$ must be an integer, so we have to calculate the closest integer number of samples that satisfy that condition as:

$$N_{sc} = \text{round} \left(\frac{\frac{f_s}{f_0}}{N_{COFDM}} \right) \quad (3.3)$$

That said, the approximated value of f_0 resulting from that calculated number of samples per chip is given by:

$$f_0 = \frac{f_s}{N_{sc} \times N_{COFDM}} \quad (3.4)$$

As previously explained in 2.3 the OFDM symbol period is usually called T_0 , and is proportional to the subcarriers spacing (f_0) as follows:

$$T_0 = \frac{1}{f_0} \quad (3.5)$$

Wich lead us to a chip time of

$$t_c = \frac{T_0}{N_{cOFDM}} \quad (3.6)$$

and that said, CP duration is now

$$T_P = t_c \times N_{c_p} \quad (3.7)$$

and the total OFDM symbol duration is

$$T_{OFDM} = T_0 + T_P \quad (3.8)$$

Since it is a discrete-time simulator, we calculated previously in Equation 3.3 the number os samples per chip (N_{sc}) that we need to sample our pseudo-continuous time signal. Knowing how much time a chip costs and the number of chip samples, they will lead us to a time resolution (the resolution of time vector samples) of:

$$d_t = \frac{t_c}{N_{sc}} \quad (3.9)$$

The total number of samples by OFDM symbol is

$$N_{sOFDM} = N_{c_T} \times N_{sc} \quad (3.10)$$

and that said, the total number simulation samples is given by

$$N_{st} = N_{sOFDM} \times N_{OFDM} \quad (3.11)$$

The time window of our simulation is defined as

$$T_W = (N_{st} - 1) \times d_t \quad (3.12)$$

and the resulting simulation time vector is given by a vector that begins with value 0 and following indexes are increased by the time resolution dt up to the time window calculated value T_W .

As the time vector is now defined, is time to define the frequency vector.

Sampling frequency is an input parameter, and the frequency resolution is given by

$$d_f = \frac{f_s}{N_{st}} \quad (3.13)$$

That said, our frequency vector is defined as a first sample that is 0, increasing the frequency resolution df up to $df \times (\frac{N_{st}}{2} - 1)$ and the other half of the vector should start in $-df \times (\frac{N_{st}}{2})$ and increase df up to df . Overall, the first half of the frequency vector should contain the frequencies from 0 to the most positive frequency, and the second half from the most negative frequency to the frequency sample before 0 defined by the resolution which is $-df$. Now that our simulation vectors are built, the simulator is ready to start the modulating process in transmitter.

3.2 Transmitter

Figure 3.2 shows the steps of OFDM modulation that goes from the actual digital bit sequence encoding to the time waveform modulated signal at the end of the transmitter antenna.

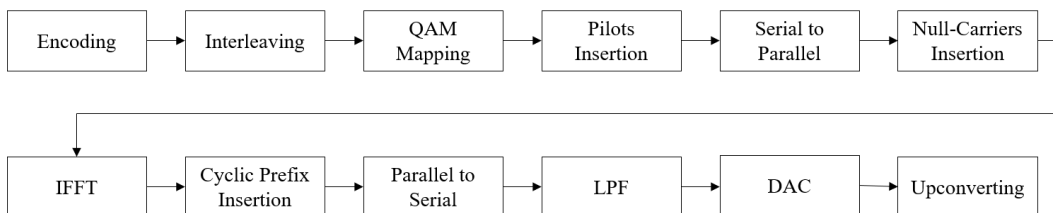


FIGURE 3.2: OFDM modulator high-level block diagram.

3.2.1 Generate Data Bits Sequence

So, the number of bits N_b that we need to generate to fulfill the number of OFDM symbols, and saving space for pilot insertion is given by:

$$N_b = N_{OFDM} \times N_{COFDM} \times (1 - p_{plt}) \times \log_2 M \quad (3.14)$$

3.2.2 Encoding

After generating the data bit sequence, the system uses a convolutional code to encode our information. It is the 1/3 tail convolutional code used in LTE systems and its encoding and decoding trellis is shown in Figure 3.3.

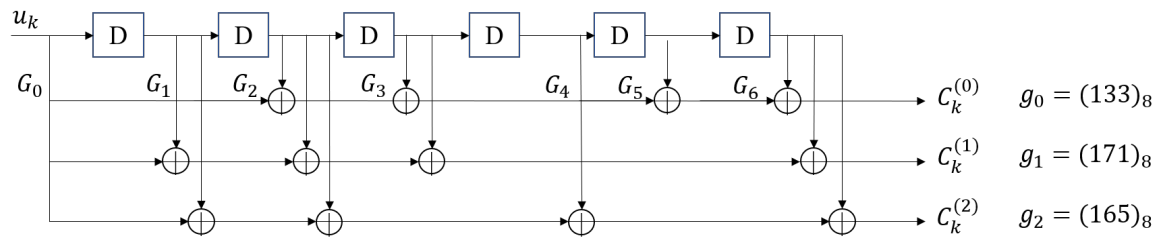


FIGURE 3.3: Encoding and Decoding Trellis of LTE systems.

For each bit that enters, it originates 3 encoded bits. Optionally, the sequence in tail padding means that it finishes with 5 zeros.

3.2.3 Interleaving

Interleaving consists of rearranging bit sequence to make the system more robust to burst errors. The MATLAB function used for interleaving was "randintrlv()" which receives a sequence of bits and rearranges them randomly.

3.2.4 M-QAM Constellation Mapping

After generating the data bit sequence, the simulator modulates it as a QAM Gray coded symbol sequence. Assuming the modulation index for the QAM modulation (M)

as an even power of 2 ($M = 2^{2n}$), and in OFDM radio systems are usually used 16-QAM, 64-QAM and 256-QAM using Grey encoding.

3.2.5 Normalize QAM Mapped Signal

After QAM modulation, we need to normalize our signal according to the normalizing factor (f_{norm}). Considering $X(f)$ the discrete non-normalized QAM modulated signal, normalizing factor is given by

$$f_{norm} = \sqrt{\frac{1}{\text{mean}(|X(f)|^2)}} \quad (3.15)$$

and normalized signal is obtain multiplying the current signal ($X(f)$) by the normalizing factor (f_{norm}) as follows:

$$X_{norm}(f) = X(f) \times f_{norm} \quad (3.16)$$

3.2.6 Add Pilot Carriers

For pilot insertion we decided to implement PSAM technique described previously in 3.3 which consists in adding pilot carriers into the OFDM discrete-frequency signal.

So, we will add a pilot in first OFDM carrier and add the subsequent pilots according to the pilot percentage (p_{plt}) defined, which do not correspond to the 5G standard frame structure. The total number of pilots is given by:

$$N_{plt} = \text{ceil}(N_{cOFDM} \times p_{plt}); \quad (3.17)$$

and the resulting number of data symbols in-between pilots (we called it gap) is given by:

$$g_{plt} = \text{floor}\left(\frac{N_{cOFDM} - N_{plt}}{N_{plt} - 1}\right) \quad (3.18)$$

So, assuming, for example, 16,384 subcarriers and a pilot percentage of 20%:

3.2.7 Serial to Parallel Conversion

The OFDM signal is modulated in parallel, which means that each simulated OFDM symbol is modulated by itself. From this section on, each step is performed to each OFDM symbol independently.

3.2.8 Insertion of Oversampling Null-Carriers

To build some space between sampling-originated spectrum repetitions, we should add some null-carriers to our frequency domain signal (zero padding). Considering a padding factor of 2, that means that we will have an IFFT size that doubles the frequency signal size, which means that we will add N_{COFDM} zeros to our N_{COFDM} sized signal.

Considering the discrete-frequency signal $X_{norm}(f)$ then our zero-padded signal is given by:

$$C_{zp}(kf) = \{C_0, \dots, C_{\frac{N_{COFDM}}{4}}, [0_1, 0_2, 0_3, \dots, 0_{N_{COFDM}}], C_{\frac{3 \times N_{COFDM}}{4}}, \dots, C_{N_{COFDM}}\} \quad (3.22)$$

where the resulting signal length is $2 \times N_{COFDM}$.

3.2.9 Inverse Discrete Fourier Transform

The rest of the OFDM modulation is in time domain, and so that, the simulator computes the inverse discrete Fourier transform (IFFT) using a fast Fourier transform algorithm. This function convertes frequency data ($C_{zp}(kf)$) into sampled time data ($c_{zp}(kt)$):

$$c_{zp}(kt) = IFFT\{C_{zp}(kf)\} \quad (3.23)$$

3.2.10 Insertion of Cyclic Prefix

As explained in 3.1, N_{c_p} is the number of CP chips and CP is a copy of the last N_{c_p} chips in the OFDM symbol, to the beggining of it. Considering the OFDM symbol time

domain sample set $c_{zp}(kt)$ the resulting set will be $c_{cp}(kt)$ with length $c_{N_{COFDM}} + N_{cp}$. For example, considering a symbol with 16 chips and $N_{cp} = 3$, the Figure 3.5 shows the resulting set of samples.

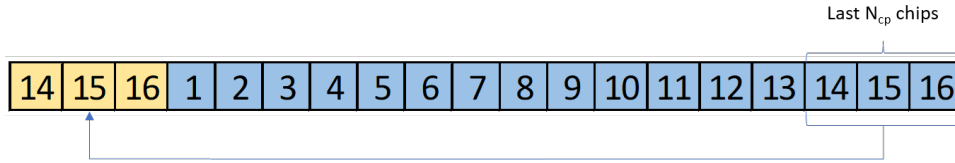


FIGURE 3.5: Example of CP insertion with $N_{COFDM} = 16$ and $N_{cp} = 3$

3.2.11 Digital to Analog Conversion

DAC consists in sampling each chip $\frac{N_{sc}}{2}$ times. Which means convoluting the symbol with a rectangular pulse with $\frac{N_{sc}}{2}$ width (Sample and Hold).

$$x_{DAC}(kt) = \text{rect}\left(\frac{kt}{\frac{N_{sc}}{2}}\right) * c_{cp}(kt) \quad (3.24)$$

3.2.12 Parallel to Serial Conversion

By the end of parallel modulation, all OFDM symbols are put back together in series.

3.2.13 Low Pass Filter

The OFDM signal before upconverting is a baseband signal. In order minimize the power spectral density of the symbol replicas generated by sampling in DAC, we've chosen to apply a perfect (rect pulse) Low-Pass Filter (LPF). Since the power information of our signal is not only in the main lobe, the filter has ratio width bigger that the OFDM bandwidth. Remember that our frequency vector (v_{freq}) is built as explained in 3.1 where it starts from 0 and grows df until the highest positive value frequency and in the middle starts with negative value frequencies and goes up until reaching $-df$. So, considering BW_{ofdm} as the OFDM signal bandwidth and $ratioBW$ the ratio between filter and OFDM signal bandwidths, we define a new frequency vector (LPF), similar in size with the v_{freq} , and between $ratioBW \times \frac{BW_{ofdm}}{2}$ and $-ratioBW \times \frac{BW_{ofdm}}{2}$ the value is 1, otherwise is 0. To filter a signal we can convolute it with the filter in time domain or multiply them in frequency domain. We've chosen to create the filter in frequency

domain as explained before, we transformed the signal back to frequency domain using Fast Fourier Transform (FFT) function, and the resulting filtered signal is given by:

$$X_{LPF} = X_{DAC} \times H_{LPF}(f) \quad (3.25)$$

An example of the effect of a LPF in the signal spectral density can be seen in Figure 3.6.

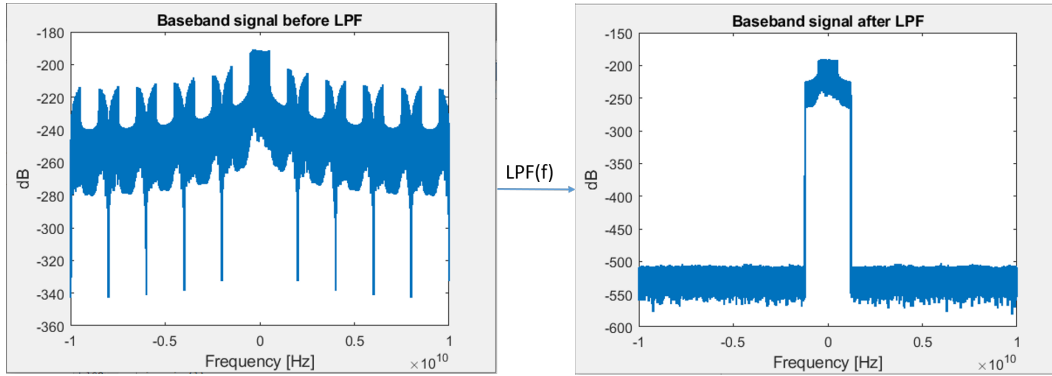


FIGURE 3.6: Example of LPF effect in signal during OFDM modulation

Now that filtering is concluded, we transform the signal back to time domain with Inverse Fast Fourier Transform (IFFT) function.

3.2.14 Upconverting to Signal Carrier

M-QAM OFDM signal is a complex signal. To guarantee a precise conversion, we need to guarantee that the specified carrier frequency (f_p) is an integer multiple of frequency resolution (df):

$$k_{fpdf} = \text{round} \left(\frac{f_p}{df} \right) \quad (3.26)$$

$$f_p = k_{fpdf} \times df \quad (3.27)$$

After that, considering $I(t)$ and $Q(t)$ the set of real and imaginary components, respectively, of our OFDM signal samples, we modulate $I(t)$ as the in-phase component and $Q(t)$ as the quadrature component.

The In-Phase Component of the OFDM signal is given by:

$$S_I(t) = I(t) \times \sqrt{2} \times \cos(2\pi f_p \times v_{time}) \quad (3.28)$$

The In-Quadrature Component of the OFDM signal is given by:

$$S_Q(t) = Q(t) \times \sqrt{2} \times \sin(2\pi f_p \times v_{time}) \quad (3.29)$$

The transmitted OFDM signal is then

$$S_{tx}(t) = S_I(t) - S_Q(t) \quad (3.30)$$

3.3 Wireless Channel

To apply one of the delay models showned in Tables 2.2, 2.3 and 2.4, considering N_{taps} as the number of taps, τ_n as the tap delay and P_n as the relative power for the n -th tap of the chosen model, we just need to generate a random gaussian amplitude ρ_n for each tap. That said, the relative powers should be normalized in order to keep the signal average power, and are given by:

$$p_n = \frac{10^{\frac{P_n}{10}}}{\sum_{n=0}^{N_{taps}-1} 10^{\frac{P_n}{10}}} \quad (3.31)$$

Considering the transmitted signal $x(t)$, the result n -th tap is given by $\rho_n \times \sqrt{p_n} \times x(t)$, and the resulting signal $y(t)$ can be described as:

$$y(t) = \sum_{n=0}^{N_{taps}-1} \rho_n \times \sqrt{p_n} \times x(t - \tau_n) \quad (3.32)$$

In the beginning of the simulation we generate a big number of channels to acquire the results of each one of them and repeat the simulation with a specific channel if we need too. Since we don't have signal information by the very beginning of the simulation,

those channels we generate are the relative powers (p_n) of each channel tap. In our simulator we decided to implement the channel models in frequency domain and in frequency domain is possible to describe this model's transfer function as a summation of exponential functions and is given by:

$$H_f(f) = \sum_{n=0}^{N_{taps}-1} \rho_n \times \sqrt{p_n} \times e^{j \cdot 2\pi f \cdot \tau_n} \quad (3.33)$$

That said, considering the transmitted signal $X(f)$, the resulting signal $Y(f)$ is given by:

$$Y(f) = X(f) \times H_f(f) \quad (3.34)$$

3.4 Additive White Gaussian Noise

In order to properly add AWGN to our signal we first need to generate random gaussian coefficients with null mean and average power of 1:

$$N_{c_{ff}}(t) = \text{randn}(1, \text{length}(y(t))) \quad (3.35)$$

The Signal-to-Noise Ratio (SNR) is specified in the beginning of the simulation, and since we can calculate the signal power, we can derivate the noise power needed to achieve that SNR.

The linear value of the SNR is given by:

$$snr = 10^{SNR/10} \quad (3.36)$$

well assuming

$$\frac{e_s}{n_o} = snr \quad (3.37)$$

and that $\frac{e_b}{n_o}$ is given by

$$\frac{e_b}{n_o} = \frac{e_s}{n_o} \times \frac{1}{\log_2 M} \quad (3.38)$$

then joining Equations 3.37 and 3.38 we have

$$\frac{e_b}{n_o} = \frac{snr}{\log_2 M} \quad (3.39)$$

That said, since

$$e_b = \frac{\text{mean}(|y(t)|^2)}{R_b} \quad (3.40)$$

joining Equations 3.39 and 3.40 we can calculate the noise unilateral Power Spectral Density (PSD), given by:

$$n_o = \frac{e_b}{\frac{e_b}{n_o}} \quad (3.41)$$

$$n_o = \frac{\frac{\text{mean}(|y(t)|^2)}{R_b}}{\frac{snr}{\log_2 M}} \quad (3.42)$$

As the AWGN noise is bilateral, the actual noise PSD is $\frac{n_o}{2}$. That said, the noise power we should add considering the full simulation sampling window is:

$$p_N = N_{PSD} \times f_s = \frac{n_o}{2} \times f_s \quad (3.43)$$

That said, the resulting noise signal is given by:

$$N_{sig}(t) = \sqrt{p_N} \times N_{cfd}(t) \quad (3.44)$$

And the resulting OFDM signal is obtained adding the channel signal to the AWGN signal:

$$X_N(t) = y(t) + N_{sig}(t) \quad (3.45)$$

3.5 Receiver

Figure 3.7 shows the steps of OFDM demodulation from the down-converting of the received signal at the receiver antenna, to equalization.

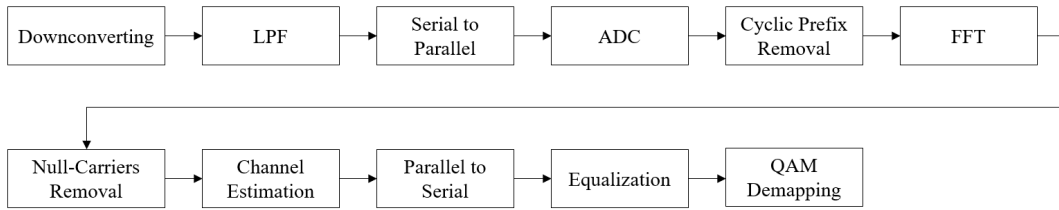


FIGURE 3.7: OFDM demodulator high-level block diagram.

3.5.1 Downconverting to Signal Carrier

At the receiver we first need to recover the separate In-Phase and In-Quadrature components.

The In-Phase Component of the OFDM signal is recovered as:

$$S_I(t) = X_{AWGN}(t) \times \sqrt{2} \times \cos(2\pi f_p \times v_{time}) \quad (3.46)$$

The In-Quadrature Component of the OFDM signal is given by:

$$S_Q(t) = X_{AWGN}(t) \times \sqrt{2} \times \sin(2\pi f_p \times v_{time}) \quad (3.47)$$

The recovered downconverted OFDM signal is then

$$S_{tx}(t) = S_I(t) - S_Q(t) \quad (3.48)$$

3.5.2 Low Pass Filter

The filtering process in receiver is the same used in transmission explained in 3.2.13.

An example of LPF effect in signal spectral density after AWGN (15dB) and a Rayleigh fading channel can be seen in Figure 3.8.

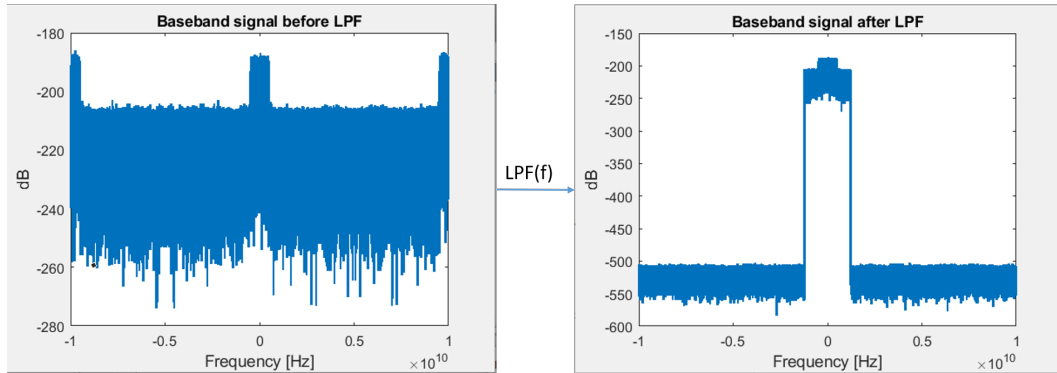


FIGURE 3.8: Example of LPF effect in signal during OFDM demodulation with SNR=15dB and over Rayleigh fading channel

3.5.3 Serial to Parallel Conversion

The OFDM signal is also demodulated in parallel. From this section on, each step is performed to each OFDM symbol independently.

3.5.4 Analog to Digital Conversion

Analog-to-Digital Converter (ADC) consists in extracting one sample of each chip. The resulting symbol will be $\frac{N_{sc}}{2}$ smaller than the received DAC symbol.

3.5.5 Removal of Cyclic Prefix

Removing the CP is simply removing the first N_{cp} samples of the downsampled OFDM symbol. Considering the CP-OFDM symbol $c_{cp}(kt)$ then after CP removal it will be $c(kt)$ with length N_{COFDM} . It is removing the additional part we have added to our signal in modulation module explained previously in 3.2.10.

3.5.6 Discrete Fourier Transform

The rest of the OFDM demodulation is back to frequency domain, and so that, the simulator computes the discrete Fourier transform (FFT) using a fast Fourier transform algorithm. This function convertes time domain data ($c(kt)$) into frequency data ($C(kf)$):

$$C(kf) = FFT\{c(kt)\} \quad (3.49)$$

3.5.7 Removal of Oversampling Null-Carriers

In 3.2.8 we explained how these null-carriers are added. This is the process to discard the samples in between the data carriers. So our symbol is again given by

$$C(f) = \{C_0, \dots, C_{\frac{N_{c_{OFDM}}}{4}}, C_{\frac{3 \times N_{c_{OFDM}}}{4}}, \dots, C_{N_{c_{OFDM}}}\} \quad (3.50)$$

where its length is again $N_{c_{OFDM}}$.

3.5.8 Channel Estimation

After removing the null carriers we are back to our discrete-frequency OFDM symbol without any samples added in the modulation process. The objective of the channel estimation is to use the pilots added to the signal, which we know the original value ($1 + 0i$) and estimate the effects of the channel, or the effects of the whole modulation process itself. The effect of a pilot transmission can be calculated by the quotient of the received amplitude and original amplitude of the pilot, as well as the quotient of received phase and original phase. The process is repeated for all considered pilot carriers to build a sequence we will further use to interpolate and equalize the estimated channel frequency response.

To make an approximated but good estimation for all simulated OFDM symbols, we compute the mean of all *pilots* sets acquired for each OFDM symbol. Then we need to estimate both amplitudes and phases separately. To do that, we compute the *interp1* function to perform an interpolation available in Matlab, which interpolates a set of samples using high level polynomials. Assuming S_{amps} and S_{phas} as the pilot sequence

interpolated amplitudes and phases, respectively, the resulting estimated channel frequency response is given by;

$$H_{est}(f) = \frac{S_{amps} \times \cos(S_{phas}) + (S_{amps} \times \sin(S_{phas})) \cdot i}{\sqrt{2}} \quad (3.51)$$

3.5.9 Parallel to Serial Conversion

By the end of parallel demodulation, all OFDM received symbols are put back together in series.

3.5.10 Equalization

The technique used to equalize the channel can differ. In case of selecting the ZF equalizer, the equalization will be made according to the equalizer (EQ) as follows:

$$E_{est} = \frac{H_{est}^*}{|H_{est}|^2} \approx \frac{1}{H_{est}} \quad (3.52)$$

In case of selecting the MMSE equalizer and considering snr as the linear value of the ratio between signal and noise power, the equalization will be made according to the equalizer (EQ_{est}) as follows:

$$E_{est} = \frac{H_{est}^*}{\frac{1}{snr} + |H_{est}|^2} \quad (3.53)$$

Chapter 4

Experimental Set-up

This chapter aims to describe the experimental system set-ups, the hardware. Note that the modulation and demodulation are executed in matlab just like the simulation process explained previously in Sections 3.2 and 3.5. Figure 4.1 illustrates a scheme of the experimental set-up.

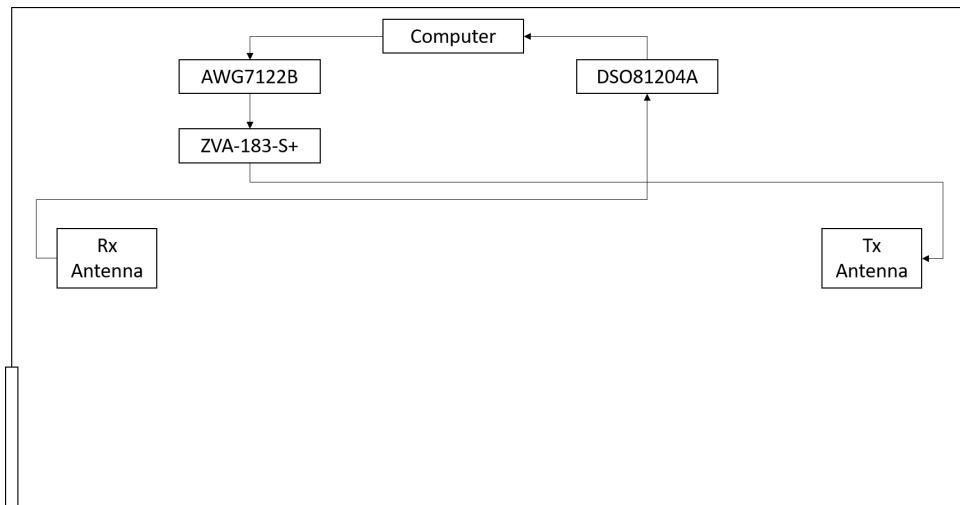


FIGURE 4.1: IT laboratory set-up scheme

To carry out the experiments we used the following hardware:

- 1 Computer with MATLAB
- 1 AWG7122B Arbitrary waveform generator
- 1 ZVA-183-S+ Eletrical amplifier:
- 2 Ultra Wideband (UWB) antennas

- 1 DSO81204A Digital storage oscilloscope

4.1 Hardware Specifications

4.1.1 AWG

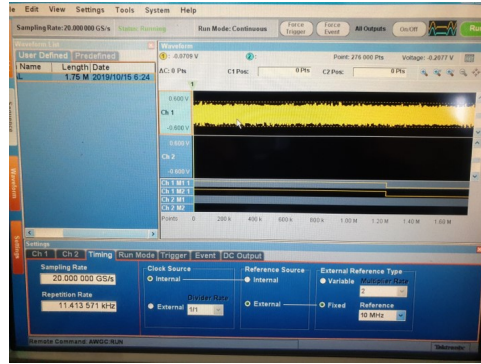


FIGURE 4.2: AWG transmitting an OFDM signal recorded with 1742300 samples

The AWG consist in an arbitrary waveform generator which we use to generate our OFDM signal. The generator has some characteristics we must consider to use it carefully, which are:

1. 24 GS/s that can be shared by two different channels at 12 GS/s each.
2. 9.6 GHz effective frequency output
3. waveform output with ± 100 ps range (1 ps resolution)
4. 8-Bit vertical resolution with two marker outputs (1mV)
5. Up to 64800000 point record length

AWG is one of the most important components of the setup, and its characteristics are translated to limitations when building a signal in MATLAB. Since it has a limited 24 GS/s, the MATLAB signal should not have a bigger sampling frequency since it must be equal to the AWG sampling frequency. That said, we decided to use a sampling frequency of 20GHz. The frequency output is related to the carrier frequencies we should use. The smaller the carrier frequency, the best signal we should acquire from AWG, so we should not get above 5GHz. Uploading MATLAB file to AWG, we can simply transmit our signal in AWG7122B and start the experiments, as illustrated in Figure 4.2

4.1.2 Amplifier

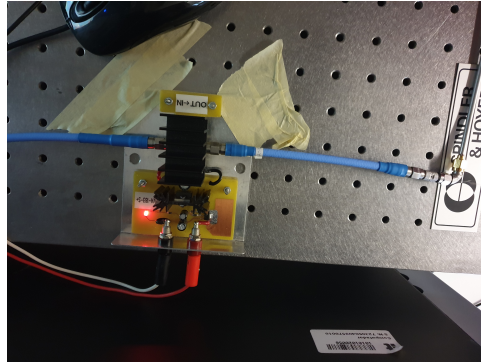


FIGURE 4.3: ZVA-183-S+ Amplifier used in wireless experimental set-up

The ZVA-183-S+ amplifier in Figure 4.3 was used to achieve greater distances since our antenna gains are small. Among the specifications of this hardware, at 25° C we must know that it operates with the following characteristics:

1. 700 MHz to 18000 MHz of frequency range
2. Typical Gain of 26 dB
3. Noise figure of 3.0 dB

This is important because we need to know which gain we should have at the transmitter antenna, and since we will carry out some tests to understand the best signal carrier frequency to perform the experimental tests, we know that we need to be in amplifier's frequency ranges so it is compatible with the system we want to test.

4.1.3 Antennas

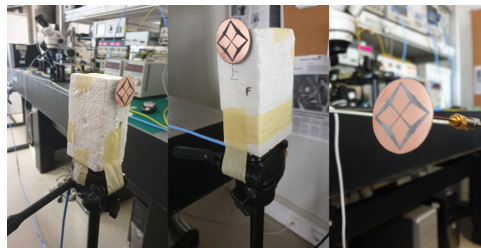


FIGURE 4.4: Antenna used in wireless experimental set-up

Figure 4.4 shows the antennas used in the wireless set-ups, they were fabricated by Instituto de Telecomunicações (IT) and we know their characteristics are the following [28]:

1. 3.1 – 10.5 GHz effective frequency output
2. around 2 dB gain at 3.5 GHz and a maximum 5 dB at 8.2 GHz

Since the antennas have a limited effective frequency output, we should consider using signal carriers at that range. The gain of the antennas is low, so we must experience a weak signal for small distances. This was the reason why we considered using a signal amplifier.

4.1.4 DSO

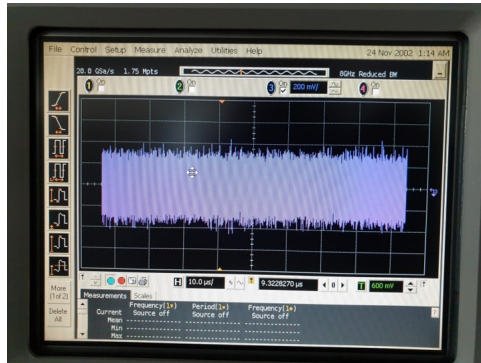


FIGURE 4.5: DSO receiving an OFDM signal recorded with 1742300 samples

The DSO consist in an digital storage oscilloscope which we use to store the data as a receiver. This oscilloscope also has some characteristics we must consider, which are:

1. 40 GS/s
2. 2000000 maximum samples storage

The DSO is the most limiting hardware when it comes to the builded signal constraints. Sampling frequency is not a problem since AWG has set it under 24 GS/s, but when it comes to the samples storage, it limited us to build a signal with less than 2000000 waveform data points, which is 32.4 times smaller than the supported record

length of AWG. This limitation only allow us to send 5 OFDM symbols which is a low number of symbols to evaluate the performance over time. The received signal in DSO81204A is recorded as shown in Figure 4.5 and sent to the computer.

4.2 Set-ups Overview

The experiments were performed in three different laboratory set-ups: back-to-back, non-amplified wireless and amplified wireless. In the first testing stage we acquired the results on a wire transmission, which allows us to check if the system is working correctly by analysing the demodulated constellation and calculating EVM (Back-to-Back set-up illustrated in Figure 4.6).

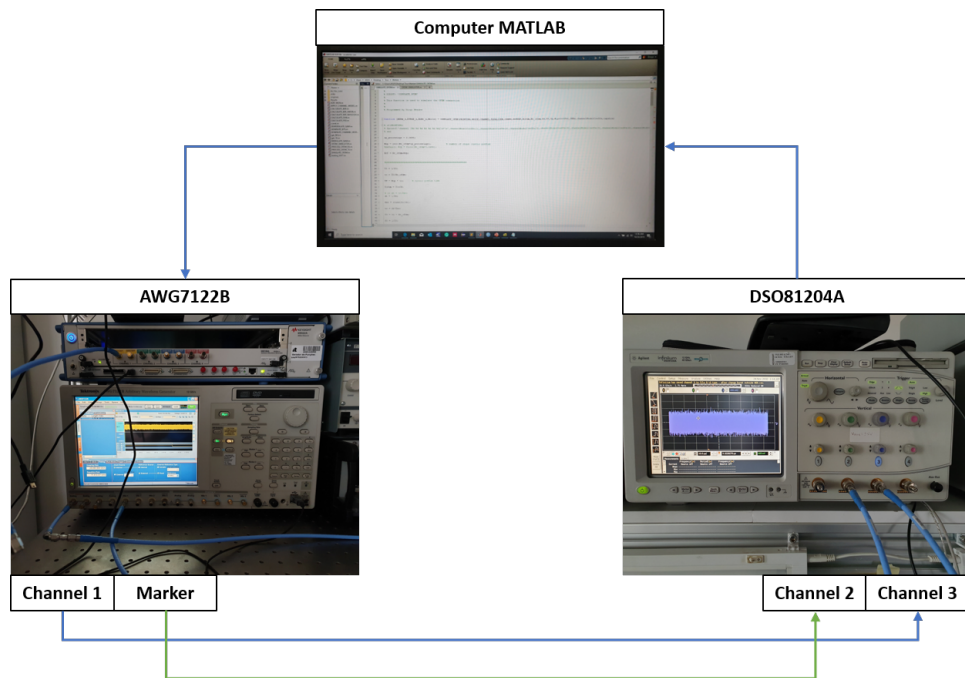


FIGURE 4.6: Back-to-Back system diagram

Second stage is a non-amplified wireless set-up where we used the antennas to connect the AWG to DSO, as illustrated in Figure 4.7.

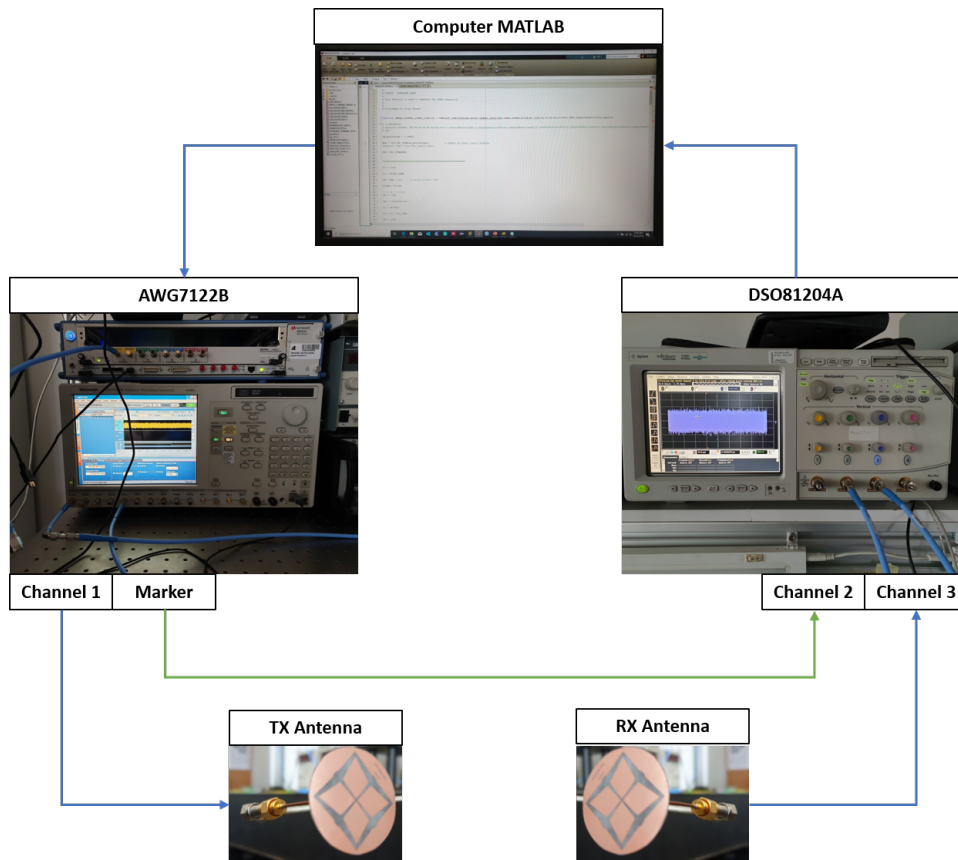


FIGURE 4.7: Simplified antennas system diagram

Third stage is an amplified wireless set-up where we used an ZVA-183-S+ amplifier between AWG and transmitter antenna to give our signal a power boost as illustrated in Figure 4.8.

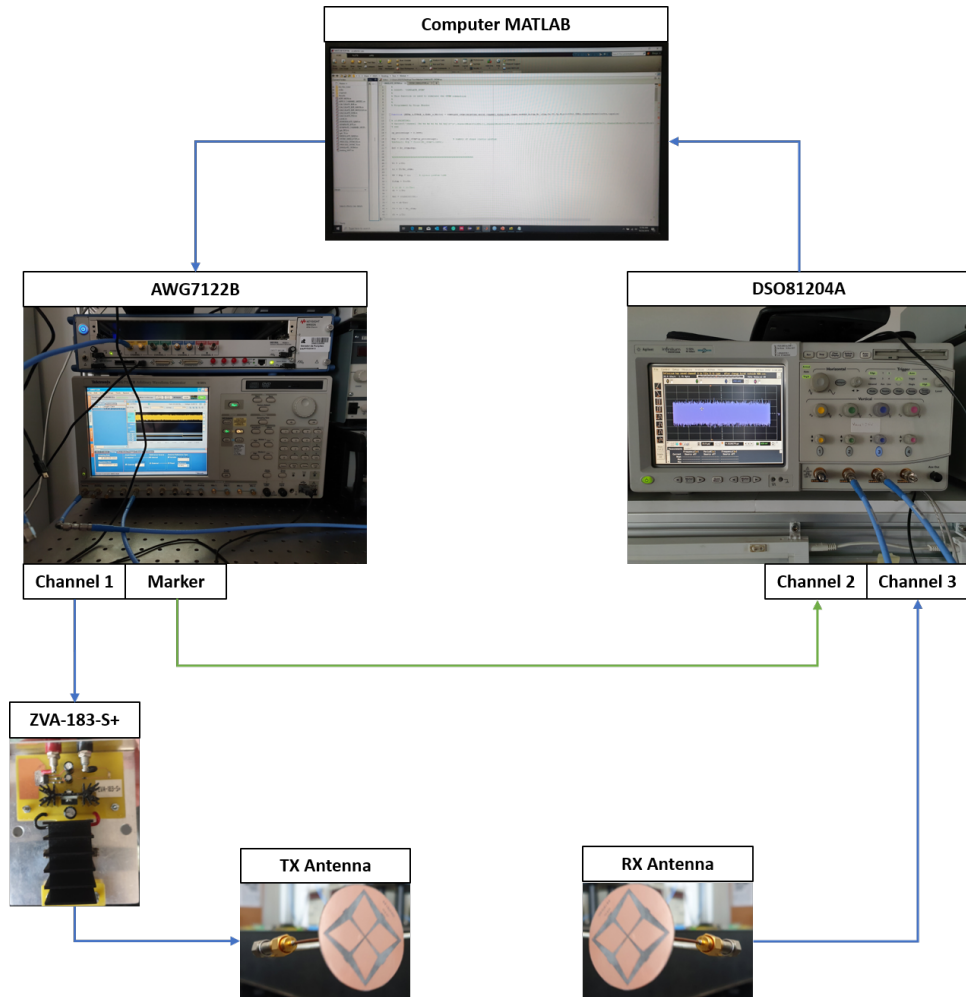


FIGURE 4.8: Amplified antennas system diagram

4.3 Offline Synchronism

In the experiments, the AWG needs a trigger to know when to start transmitting the signal. This signal is transmitted, reaches the DSO and by the time it is back to the computer, the signal presents a time-shift. This asynchronism is treated by a MATLAB function named "correl" which performs a basic correlation between two input signals resulting in the received index of the first original sample and the final synchronised signal. Assuming stx and srx has the original and received signals in the time domain, respectively, the correlation is performed in the four following steps:

1. Passing original signal to frequency domain - $Stx = \text{FFT}\{|stx|\}$
2. Passing received signal to frequency domain - $Srx = \text{FFT}\{|srx|\}$

3. Multiplying the conjugate of Srx and Stx - $S_{corr} = Srx^* \times Stx$
4. Passing the resulting correlation sequence to time-domain - $s_{corr} = \text{IFFT}\{S_{corr}\}$

The maximum value of the obtained correlated sequence s_{corr} represents the value that is at the most reliable shift index. That means that identifying the index of the maximum value, we can shift the received signal and the synchronism is established.

Chapter 5

Results

This chapter aims to describe the simulation/experimental results and their analysis. Consider that the results presented in this dissertation are the best obtained within a given scenario.

5.1 Simulation Performance

The simulation scenario is described in Table 5.1.

TABLE 5.1: OFDM Simulation Signal Parameters

Parameter	Value
Signal to Noise Ratio	0-25 0-30 dB
Number of Symbols	50
Number of Subcarriers	16384
M-QAM Index	64 256
Signal Carrier Frequency	5 GHz
Sampling Frequency	20 GS/s
Subcarrier Spacing	60 kHz
Symbol Duration	16.67 us
Cyclic Prefix Duration	1.16 us
FFT Size	32768
Signal Bandwidth	1 GHz
Pilot Percentage	20 %

The number of bits simulated depends on the QAM order and if the information is encoded. Table 5.2 shows the variation of the number of simulated bits as the resulting minimal BER we can achieve.

TABLE 5.2: Simulation number of bits and minimum achievable BER in each simulation

Modulation	Code scenario	#Bits	Minimum achievable BER
64-QAM	Uncoded	3931200	2.544×10^{-7}
64-QAM	Hard Decision	1310394	7.631×10^{-7}
256-QAM	Uncoded	5241600	1.908×10^{-7}
256-QAM	Hard Decision	1747194	5.724×10^{-7}

5.1.1 AWGN Channel Performance

In order to evaluate if the AWGN channel is correctly induced to our system, we need to obtain the results and compare them to the theoretical BER performance. The formula used to the theoretical results of BER, is the formula of M-QAM probability of error and is given by:

$$BER_{theoretical} = 2 \times \frac{1 - \frac{1}{\sqrt{M}}}{\log_2 M} \times \text{erfc} \left(\sqrt{\frac{3 \times \log_2 \sqrt{M}}{M - 1} \times \frac{snr}{\log_2 M}} \right) \quad (5.1)$$

Figures 5.1 and 5.2 show the BER performance and EVM performance for different SNR values.

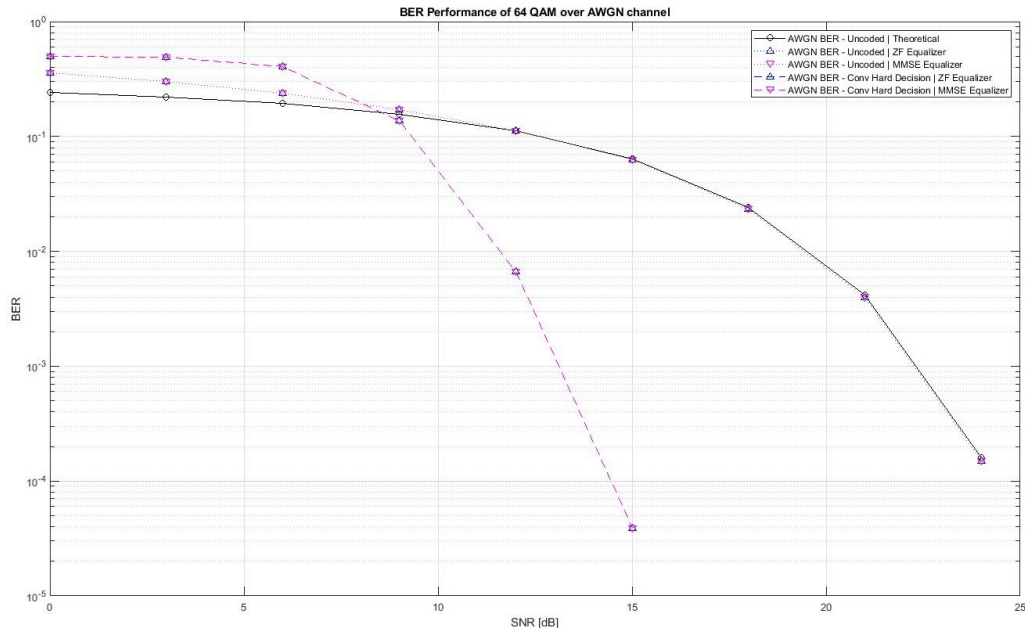


FIGURE 5.1: 64-QAM simulation performance over AWGN channel

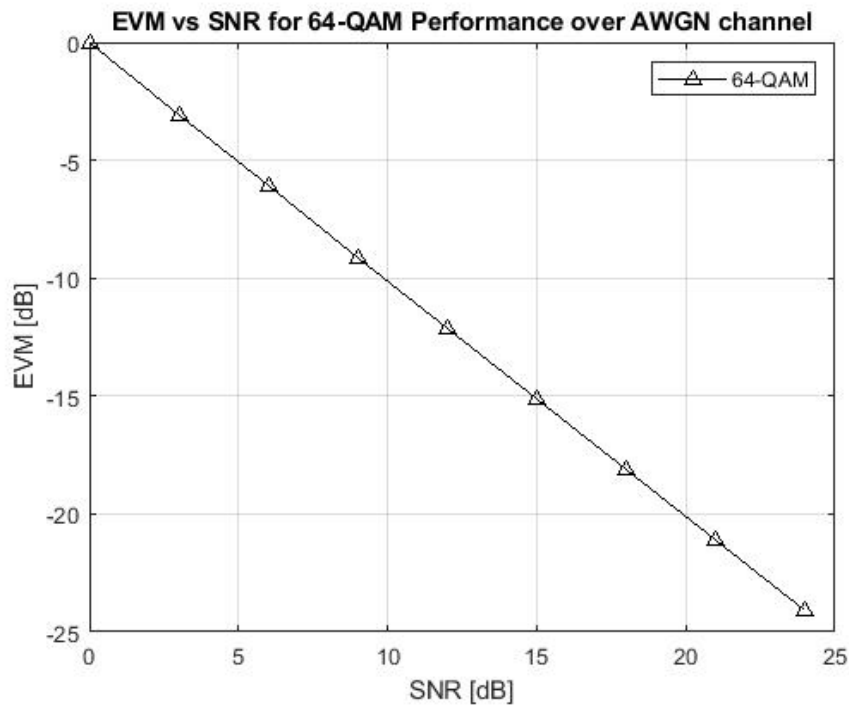


FIGURE 5.2: 64-QAM EVM vs SNR over AWGN channel

As expected, the uncoded 64-QAM performance is in accordance to the theoretical one for SNR values above 12dB. Values below 12dB assume to generate only one error bit for each error symbol which can not be true when simulating many different signals over AWGN channel. In this case we also acquired the results with hard decision convolutional LTE-A code as the Forward Error Correction (FEC) code, and the lowest

BER we obtained was 3.904×10^{-5} for $SNR = 15\text{dB}$ which translates to a performance improvement over 9dB of SNR. To make sure our AWGN channel is correctly induced, we also need to acquire the EVM since theoretically it should be the inverse value of SNR or negative in logarithmic scales ($EVM \text{ [dB]} = -SNR \text{ [dB]}$).

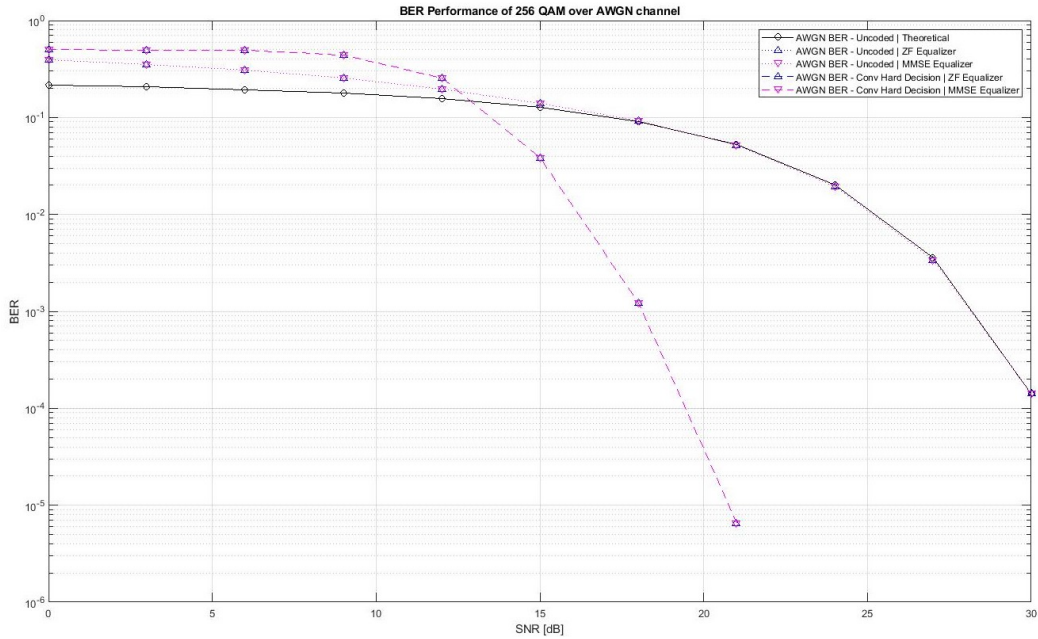


FIGURE 5.3: 256-QAM simulation performance over AWGN channel

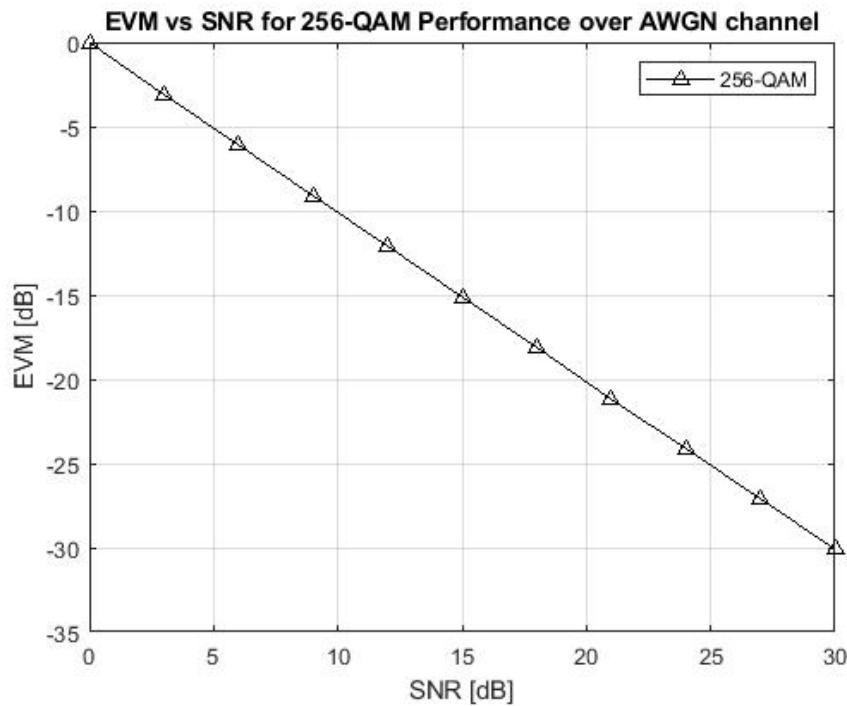


FIGURE 5.4: 256-QAM EVM vs SNR over AWGN channel

256-QAM performance is also in accordance to the theoretical performance starting

on 18dB of SNR. The FEC results show a BER of 5.540×10^{-6} for 21dB which also translates to a performance improvement over 9dB of SNR.

Since the simulated BER curves are in accordance to the theoretical ones, as the EVM results we conclude that the addition of AWGN is performed correctly.

5.1.2 Rayleigh Channel Performance

As the theoretical curves of Rayleigh channel OFDM QAM assume an infinite number of channel performances, we are not able to compare the results to the theoretical curves since we are only comparing the results of two hundred realizations of the wireless channel. In order to evaluate the reliability of the results, we can look at Figures 5.5, 5.6, 5.7 and 5.8 which demonstrate the Mean BER variance along the number of Rayleigh channel possibilities simulated to a total of 50 simulations for each scenario.

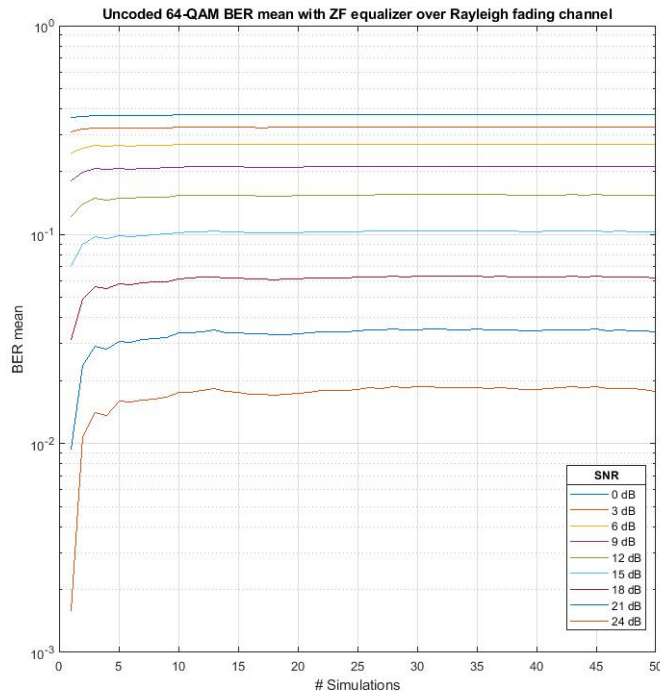


FIGURE 5.5: Uncoded 64-QAM Mean BER with ZF equalizer over Rayleigh fading channel

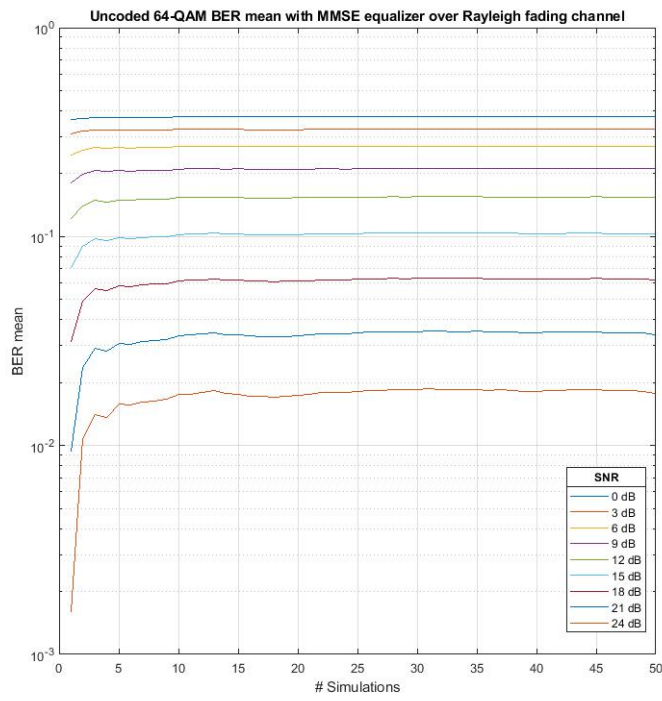


FIGURE 5.6: Uncoded 64-QAM Mean BER with MMSE equalizer over Rayleigh fading channel

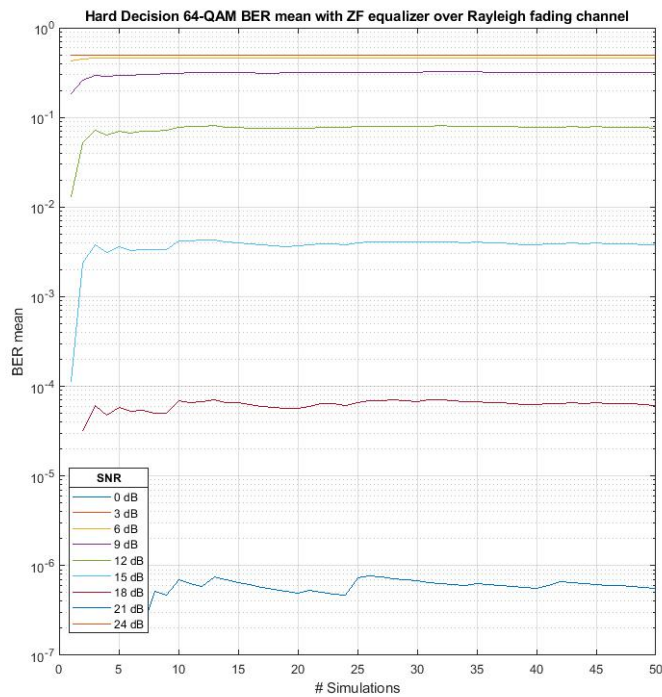


FIGURE 5.7: Hard Decision 64-QAM Mean BER with ZF equalizer over Rayleigh fading channel

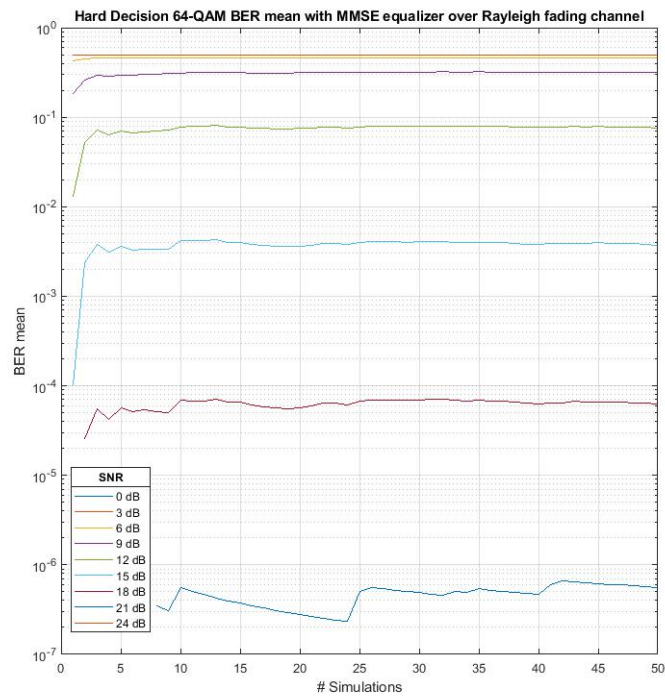


FIGURE 5.8: Hard Decision 64-QAM Mean BER with MMSE equalizer over Rayleigh fading channel

Figures 5.5, 5.6, 5.7 and 5.8 show that for 64-QAM we obtained reduced variances in Mean BER up to 24dB in Uncoded scenarios and up to 21dB in hard decision scenarios. So we decided to perform the tests with 50 channel simulations and get reliable results up to 21 dB of SNR.

Figures 5.9, 5.10, 5.11 and 5.12 show the results of the repeated process, this time for 256-QAM.

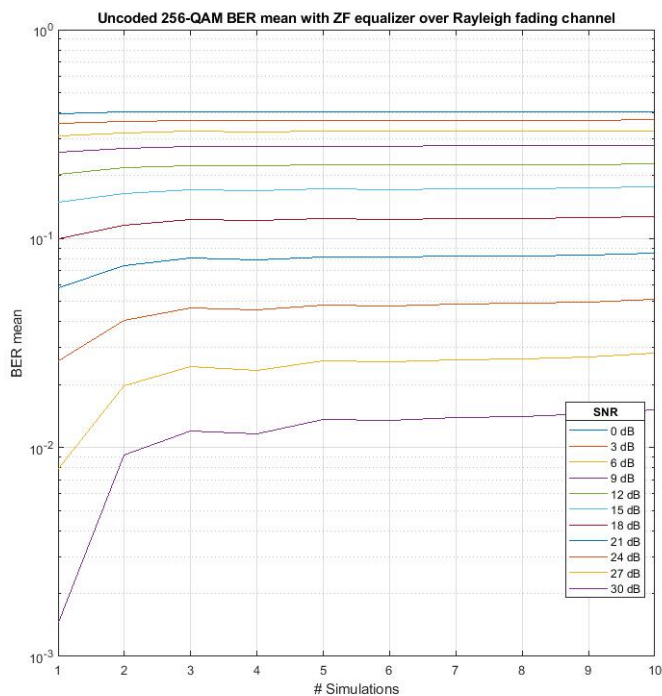


FIGURE 5.9: Uncoded 256-QAM Mean BER with ZF equalizer over Rayleigh fading channel

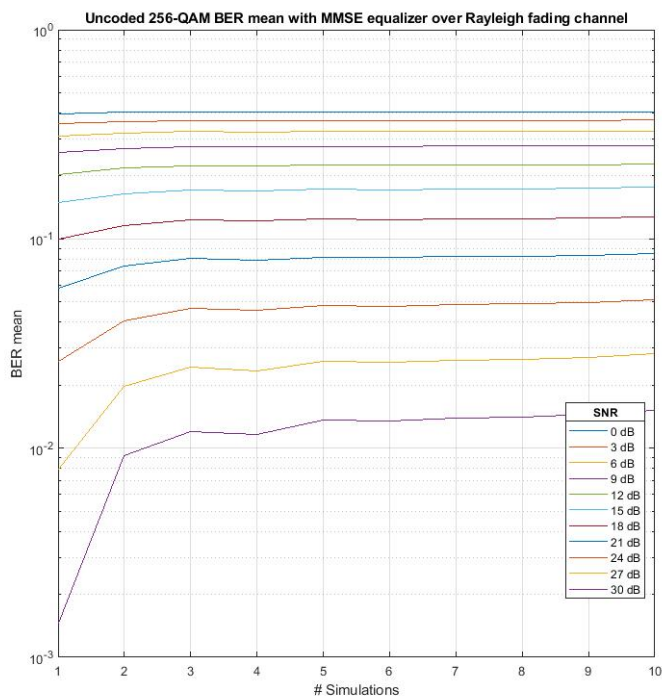


FIGURE 5.10: Uncoded 256-QAM Mean BER with MMSE equalizer over Rayleigh fading channel

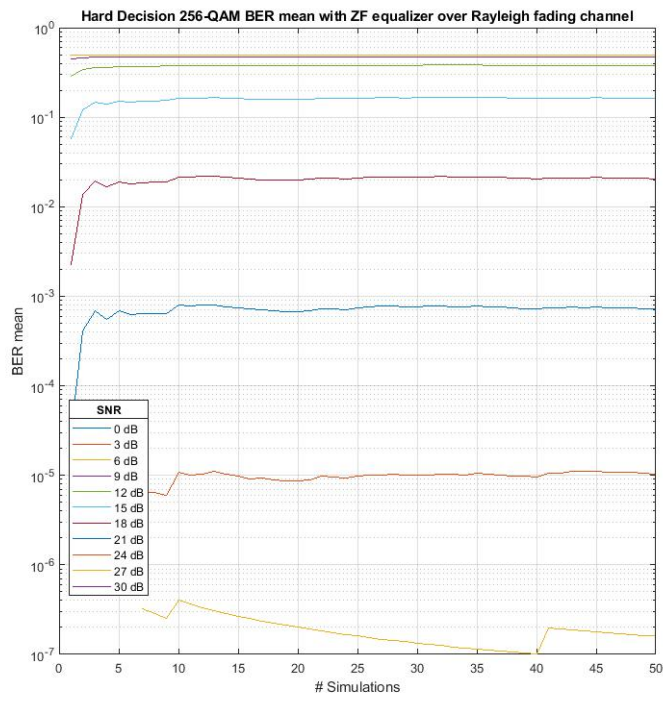


FIGURE 5.11: Hard Decision 256-QAM Mean BER with ZF equalizer over Rayleigh fading channel

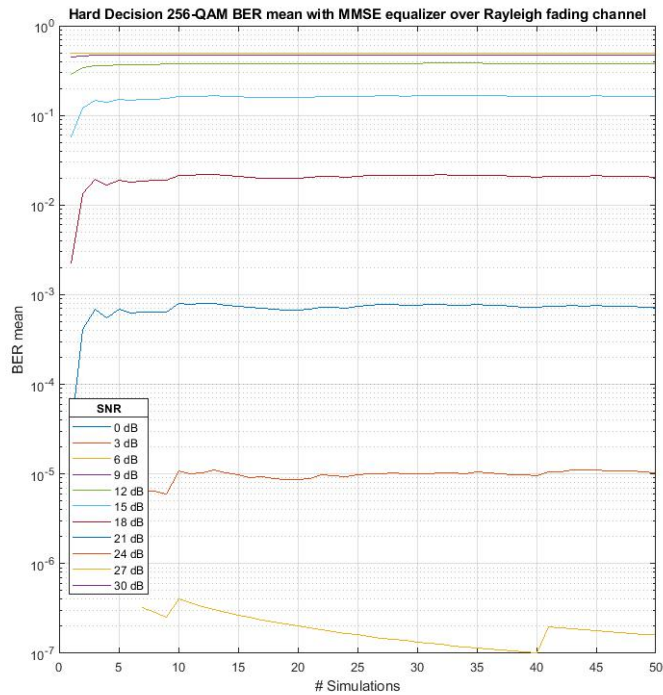


FIGURE 5.12: Hard Decision 256-QAM Mean BER with MMSE equalizer over Rayleigh fading channel

For 256-QAM we obtained reduced variances in Mean BER up to 30dB in Uncoded scenarios and up to 24dB in hard decision scenarios. So we decided to perform the tests with the same 50 channel simulations and get reliable results up to 24dB of SNR. Overall, no noticed changes between ZF and MMSE equalizers performance in our system. The bigger the SNR, the closer should the performances be, although, even for small values of SNR, the performance is quite the same.

That being said, Figures 5.13 and 5.15 show the performance of 64-QAM and 256-QAM over Rayleigh fading channels, respectively.

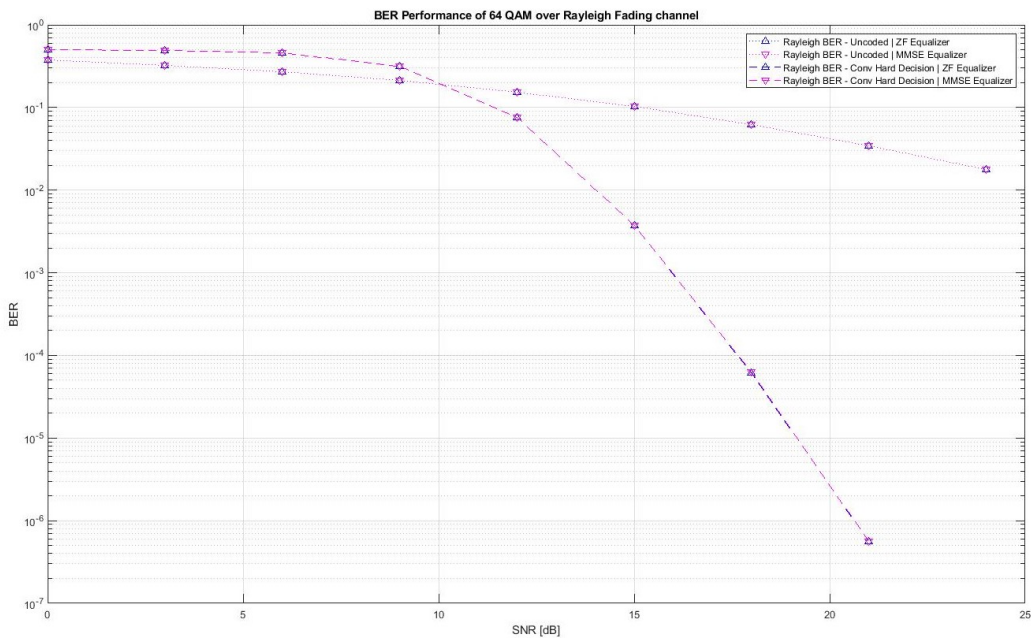


FIGURE 5.13: 64-QAM simulation performance over Rayleigh fading channel

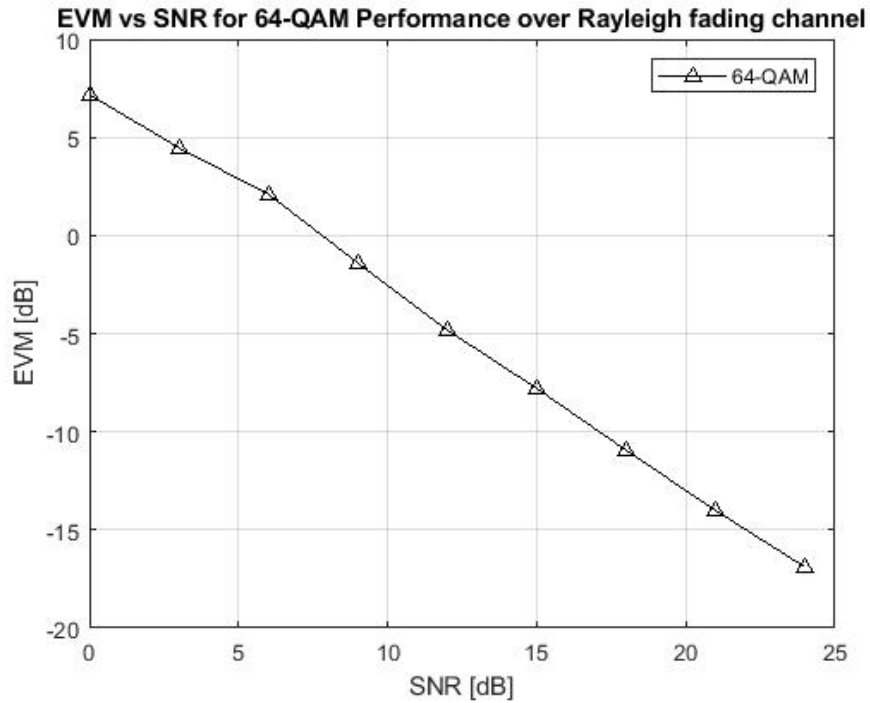


FIGURE 5.14: 64-QAM EVM vs SNR over Rayleigh fading channel

The behaviour of 64-QAM BER over SNR seems to have a correct behaviour, which means a dropping curve generating an EVM decreasing linearly with SNR, and stable over 50 simulations. The lowest 64-QAM BER we obtained from the simulation was 5.581×10^{-7} for 21dB of SNR which translates to a BER that is 10^5 smaller than the uncoded BER for same SNR value.

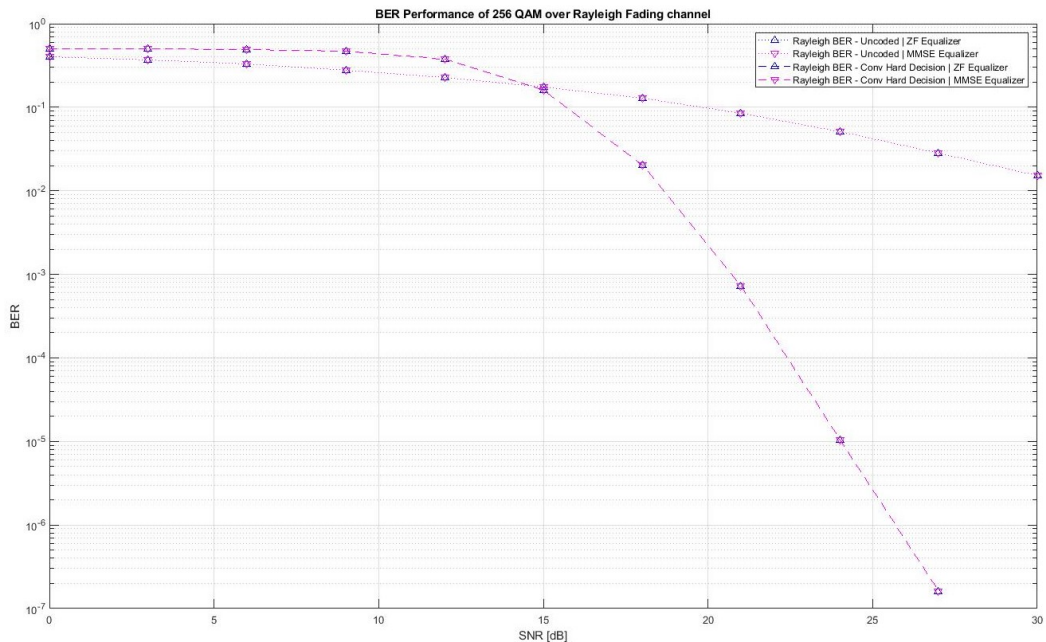


FIGURE 5.15: 256-QAM simulation performance over Rayleigh fading channel

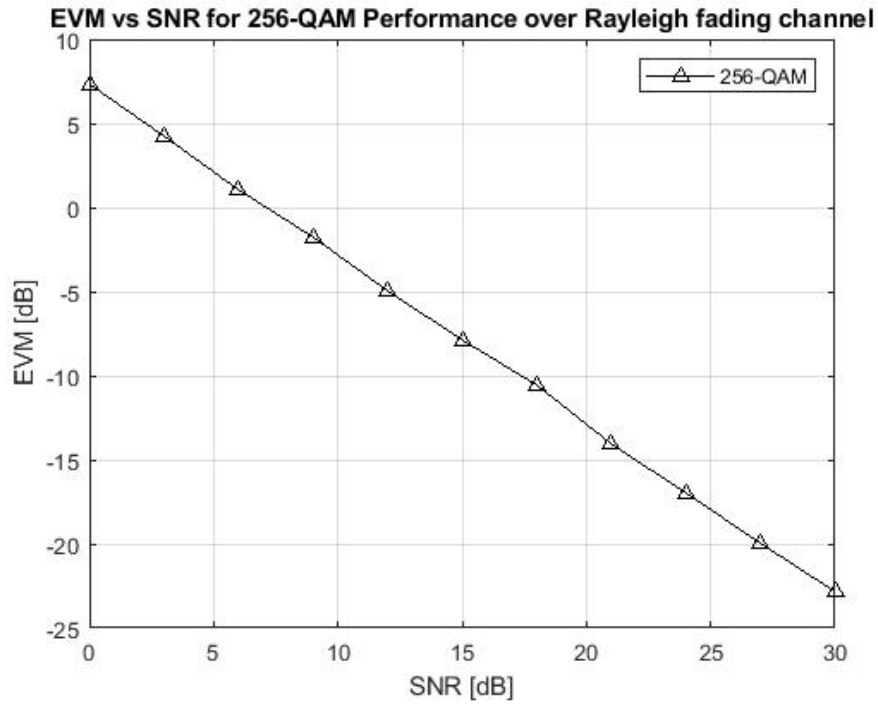


FIGURE 5.16: 256-QAM EVM vs SNR over Rayleigh fading channel

The behaviour of 256-QAM is similar with the 64-QAM with a penalty around 5 dB. The lowest 256-QAM BER we obtained from the simulation was 1.603×10^{-7} for 27dB of SNR which also translates to a 10^5 smaller BER than the uncoded BER for same SNR value.

5.2 Experimental Performance

The experimental scenario is described in Table 5.3.

TABLE 5.3: OFDM Experimental signal Parameters

Parameter	Value
Number of Symbols	5
Number of Subcarriers	16384
M-QAM Index	64 256
Sampling Frequency	20 GS/s
Subcarrier Spacing	60 kHz
Symbol Duration	16.67 us
Cyclic Prefix Duration	1.16 us
FFT Size	32768
Signal Bandwidth	1 GHz
Pilot Percentage	20 %

The number of bits simulated depends on the QAM order and if the information is encoded. Table 5.4 shows the variation of the number of simulated bits as the consequent minimum BER we can achieve.

TABLE 5.4: Experimental number of bits and achievable BER

Modulation	Code scenario	#Bits	Minimum achievable BER
64-QAM	Uncoded	393120	2.544×10^{-6}
64-QAM	Hard Decision	131034	7.632×10^{-6}
256-QAM	Uncoded	524160	1.908×10^{-6}
256-QAM	Hard Decision	174714	5.724×10^{-6}

Table 5.5 shows the effective data rates for each experimental scenario.

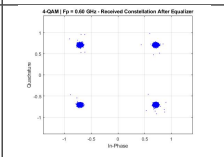
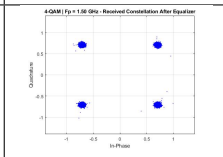
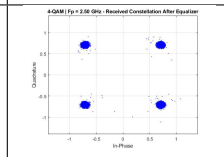
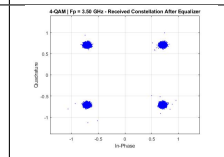
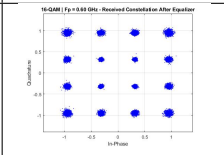
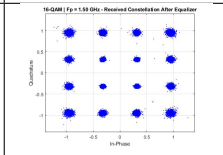
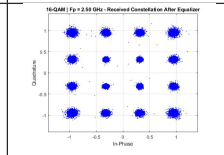
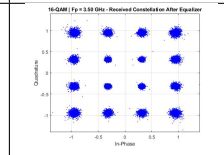
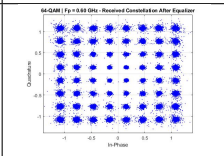
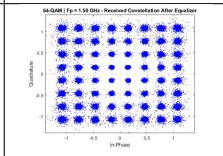
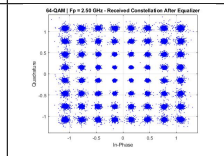
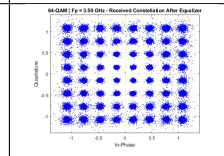
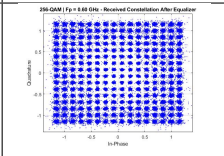
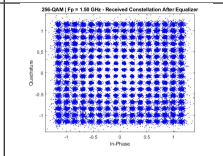
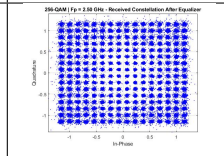
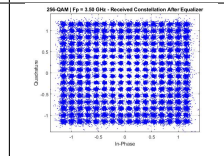
TABLE 5.5: Effective data rates for each considered scenario

Modulation	Code scenario	Effective Data Rate
64-QAM	Uncoded	4.4 Gbps
64-QAM	Hard Decision	1.5 Gbps
256-QAM	Uncoded	5.9 Gbps
256-QAM	Hard Decision	2.0 Gbps

5.2.1 AWG Effective Frequency in Back-to-Back

As a test bed of the transceiver experimental set-up, Table 5.6 presents the constellation obtained over different scenarios of modulation (from 4 to 256 QAM) and Figures 5.17 and 5.18 show us the EVM and BER performance of the AWG over different signal carriers, which depend on its frequency selective response.

TABLE 5.6: Test Bed AWG constellations comparison between 4/16/64/256 QAM on 0.6/1.5/2.5/3.5 GHz of carrier frequency

M/Fp	0.6 GHz	1.5 GHz	2.5 GHz	3.5 GHz
4-QAM				
16-QAM				
64-QAM				
256-QAM				

The constellations obtained are not perfect, and those imperfections might be generated by the hardware or the simulator itself. Unfortunately, no studies were carried out to understand this behaviour for the lack of time of laboratory availability.

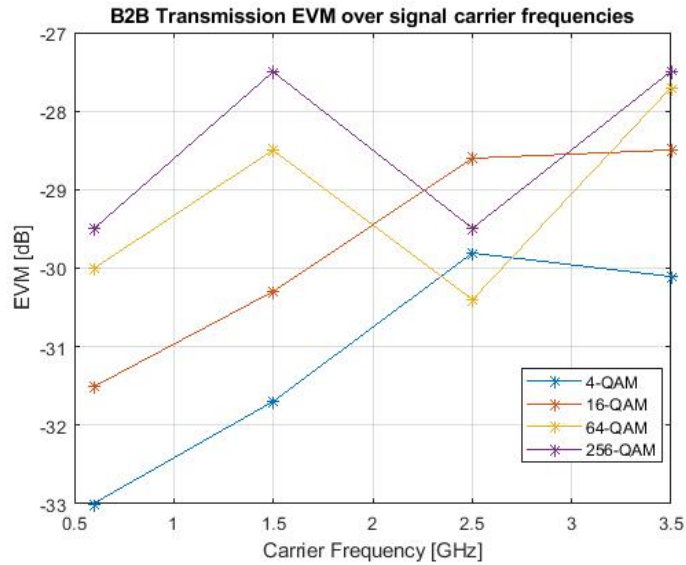


FIGURE 5.17: Test Bed AWG EVM performance comparison between 4/16/64/256 QAM on 0.6/1.5/2.5/3.5 GHz of carrier frequency

Figure 5.17 shows the EVM over signal frequencies. There is a clear improvement from 0.5 GHz to the higher carriers and 2.5 GHz seems to be the best when it comes to the homogenesis of the results. In spite of being the carrier frequency that shows the most accurate results and the lowest results for 64 and 256 QAM, all the frequencies here tested seem to be useful.

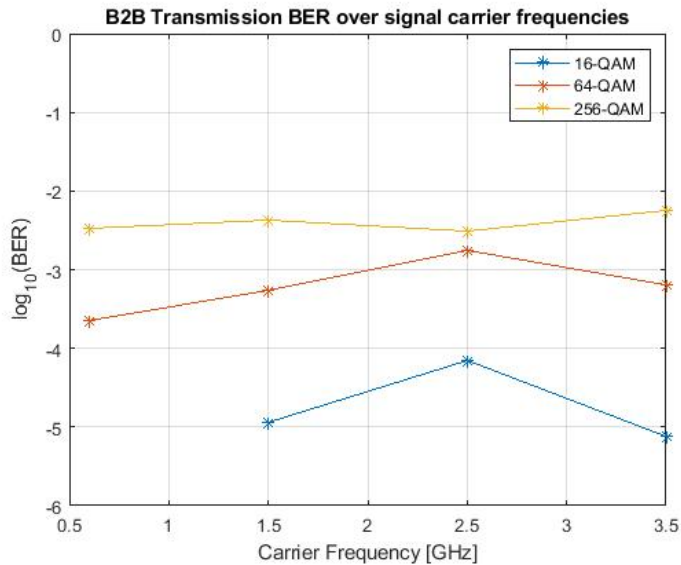


FIGURE 5.18: Test Bed AWG BER performance comparison between 4/16/64/256 QAM on 0.6/1.5/2.5/3.5 GHz of carrier frequency

Note that for the entire 4-QAM BER plot and 16-QAM at 0.6 GHz there is no data since the results were below the minimum measurable BER, and wouldn't be fair to

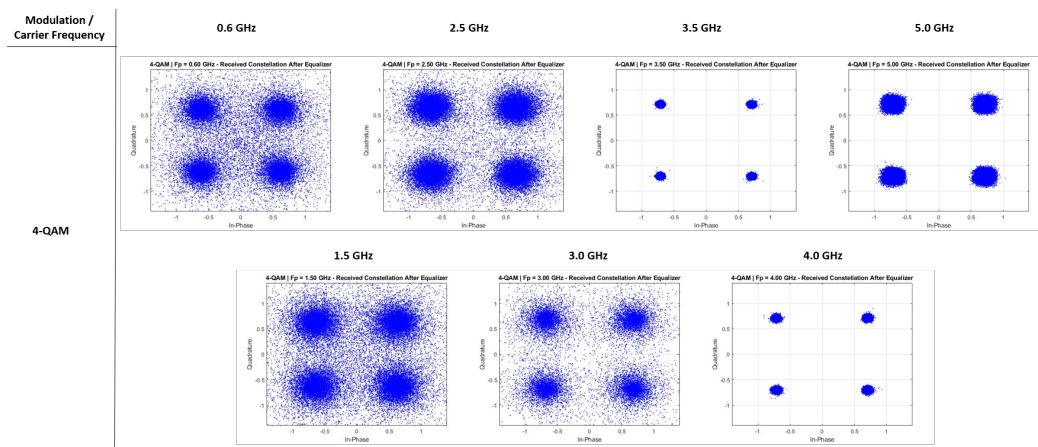
assume the minimum value as the result of that measurement. BER over frequencies is stable and does not seem to show an overcoming frequency. Overall, we can not conclude which carrier frequency is the best one to use, and so we need to perform the same tests to the antennas since AWG does not seem to limitate our system in this specific feature.

5.2.2 Non-Amplified Wireless

5.2.2.1 Antennas Effective Frequency

In the wireless scenario, is also important to analyse the frequency selective response of the antennas. To do that, we transmitted the OFDM signal with 4-QAM modulation over 0.6/1.5/2.5/3.0/3.5/4.0/5.0 GHz as carrier frequency at a minimal distance of 1.5cm to get the best results possible. The results are shown in Table 5.7.

TABLE 5.7: Test Bed antennas received 4-QAM constellations comparison between 0.6/1.5/2.5/3.0/3.5/4.0/5.0 GHz of carrier frequency



Just looking at the constellation is clear that 3.5 GHz and 4.0 GHz show the best results, which means that the recovered constellation is way more close to the original constellation than the others. The resulting EVM values and performance over signal frequency carriers for 4-QAM is presented in Figure 5.19.

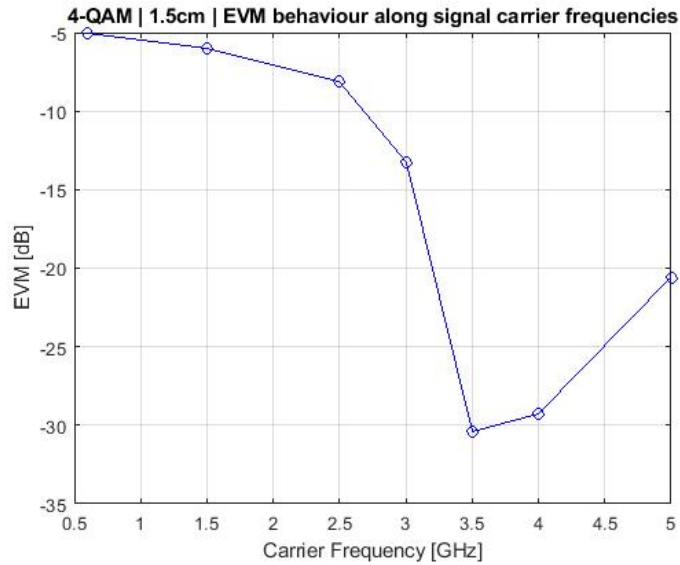


FIGURE 5.19: Test Bed antennas measured 4-QAM EVM over carrier frequency

In Figure 5.19, we can see an approximated transfer function of the antennas, which mean that the antennas gain and performance is way better in 3.5GHz-4.0GHz range than it is outside that range. The best EVM obtained was at 3.5GHz and is a suitable frequency to use in the system. Since the EVM limitation of AWG does not vary significantly from 3.5GHz to 4.0GHz, antennas are the limiting factor here, and we considered to use the best EVM performer which is the 3.5 GHz.

Now that we tested the best suitable signal carrier to use with AWG and the antennas, it is time to measure the EVM and BER performance along distance between antennas.

5.2.2.2 Performance along Distance

Since the antennas present a reduced gain, our distance tests will be carrier from 1.5cm to 45.5cm with consecutive gaps of 11.0cm, EVM and BER performance along distance are shown in Figures 5.20 and 5.21.

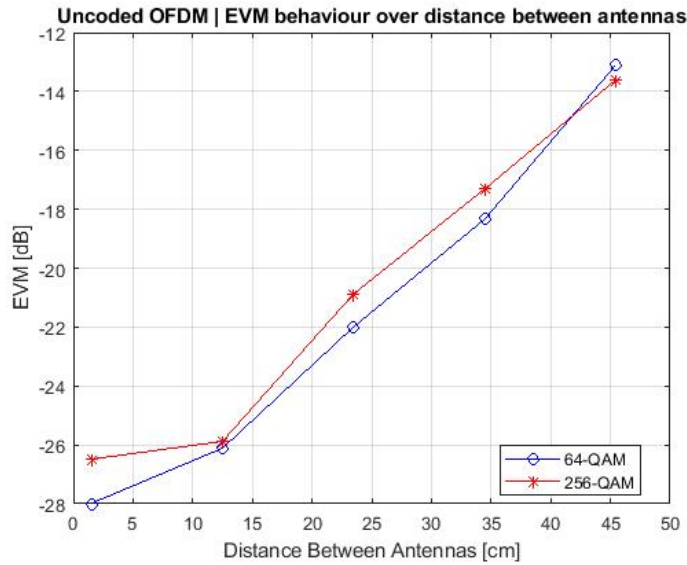


FIGURE 5.20: Uncoded 64/256 QAM EVM Performance along distance without amplification

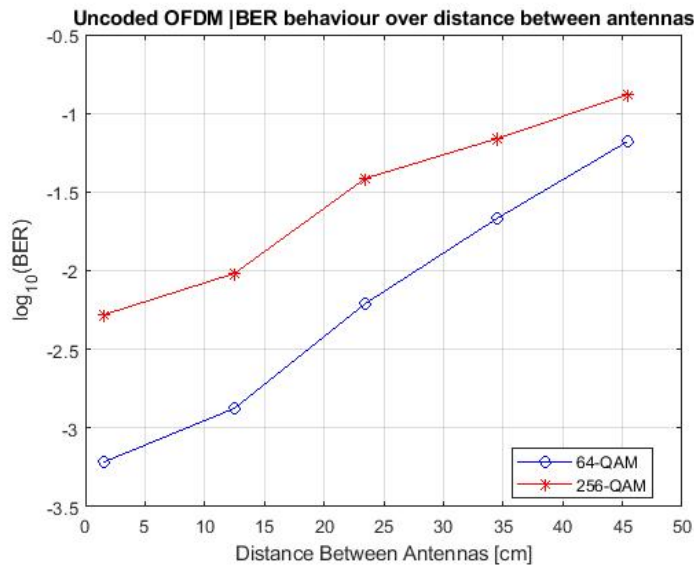


FIGURE 5.21: Uncoded 64/256 QAM BER Performance along distance without amplification

As expected, EVM and BER performance decreases with the increase of distance between antennas. From 1.5cm to 45.5cm EVM increases 15dB for 64-QAM and 13dB for 256-QAM and BER grows from 6.029×10^{-4} to 6.670×10^{-2} in 64-QAM and from 5.205×10^{-3} to 1.313×10^{-1} . Curiously, EVM of 64-QAM seems to decrease more from 1.5cm to 11.5cm and from 34.5cm to 45.5cm than it does in the middle measured gaps, when 256-QAM shows the opposite behaviour having an accentuated decrease from 11.5cm to 45.5cm but from 1.5cm to 11.5 the decrease is way lower. Laboratory conditions were

not the best to perform these tests since there are many objects inside the room, these objects can reflect the signal and cause variations in EVM we can only predict using a powerful ray tracing tool which we do not have access to.

Tables 5.8,5.9,5.10,5.11 and 5.12 show all the measurements made for each distance depending on QAM modulation order and the encoding scenario.

TABLE 5.8: BER Comparison between modulation and encoding scenarios for 1.5cm

Modulation	Encoding Scenario	EVM [dB]	Measured BER	Simulated BER
64-QAM	Uncoded	-28.0	6.029×10^{-4}	$< 1.782 \times 10^{-2}$
64-QAM	Hard Decision	-27.7	$< 7.632 \times 10^{-6}$	$< 5.581 \times 10^{-7}$
256-QAM	Uncoded	-27.8	5.205×10^{-3}	$< 1.516 \times 10^{-2}$
256-QAM	Hard Decision	-26.5	$< 5.724 \times 10^{-6}$	$< 1.603 \times 10^{-7}$

TABLE 5.9: BER Comparison between modulation and encoding scenarios for 12.5cm

Modulation	Encoding Scenario	EVM [dB]	Measured BER	Simulated BER
64-QAM	Uncoded	-26.1	1.325×10^{-3}	$< 1.782 \times 10^{-2}$
64-QAM	Hard Decision	-26.3	$< 7.632 \times 10^{-6}$	$< 5.581 \times 10^{-7}$
256-QAM	Uncoded	-25.9	9.627×10^{-3}	$< 1.516 \times 10^{-2}$
256-QAM	Hard Decision	-24.7	$< 5.724 \times 10^{-6}$	$< 1.603 \times 10^{-7}$

TABLE 5.10: BER Comparison between modulation and encoding scenarios for 23.5cm

Modulation	Encoding Scenario	EVM [dB]	Measured BER	Simulated BER
64-QAM	Uncoded	-22.0	6.110×10^{-3}	$< 1.782 \times 10^{-2}$
64-QAM	Hard Decision	-22.1	$< 7.632 \times 10^{-6}$	$< 5.581 \times 10^{-7}$
256-QAM	Uncoded	-20.9	3.828×10^{-2}	2.580×10^{-2}
256-QAM	Hard Decision	-20.8	$< 5.724 \times 10^{-6}$	$< 1.603 \times 10^{-7}$

TABLE 5.11: BER Comparison between modulation and encoding scenarios for 34.5cm

Modulation	Encoding Scenario	EVM [dB]	Measured BER	Simulated BER
64-QAM	Uncoded	-18.3	2.159×10^{-2}	$< 1.782 \times 10^{-2}$
64-QAM	Hard Decision	-19.4	$< 7.632 \times 10^{-6}$	$< 5.581 \times 10^{-7}$
256-QAM	Uncoded	-17.3	6.910×10^{-2}	5.001×10^{-2}
256-QAM	Hard Decision	-17.4	1.603×10^{-4}	9.889×10^{-6}

TABLE 5.12: BER Comparison between modulation and encoding scenarios for 45.5cm

Modulation	Encoding Scenario	EVM [dB]	Measured BER	Simulated BER
64-QAM	Uncoded	-13.1	6.670×10^{-2}	3.606×10^{-2}
64-QAM	Hard Decision	-14.3	$< 7.632 \times 10^{-6}$	$< 5.581 \times 10^{-7}$
256-QAM	Uncoded	-13.6	1.313×10^{-1}	8.991×10^{-2}
256-QAM	Hard Decision	-13.1	3.240×10^{-2}	8.524×10^{-4}

The measured values that present the "less than" ($<$) values, they mean that our twenty realizations of the channel had a result of $BER = 0.0$ which means that we have no errors and we can only conclude that it is lower than the minimum BER we can simulate as shown previously in Table 5.4. Simulated BER was obtained by getting the SNR which generates the specific labeled EVM at Figures 5.14 and 5.16. Some of those simulated results also show the same "less than" symbol which means that there are no simulated results that allow us to identify the SNR that generates the needed EVM value. We can only conclude that the greater simulated SNR value, the smaller the BER, and the simulated BER is smaller than the last simulated BER, which can be seen in Figures 5.13 and 5.15. Overall, the results are close to the simulated values, and the decreasing EVM and BER along distance is notable.

It is hard to look at EVM and BER performance values and understand if those results have an expected behaviour since the laboratory has a lot of equipment that can reflect the signal. To understand that, we assumed that our system should be at least compared to a six-rays system model. That said, Figure 5.22 shows the measured path loss values and the theoretical path losses of 3 different models: free-space model, two-ray model with perfect ground ($\Gamma = -1$) and six-rays model with perfect ground (considering that the antennas are in the middle of the room, equally distant from the walls and with a clear LoS). The measured path loss is obtained by the subtraction of the received signal power (in dB) by the transmitted signal power (in dB).

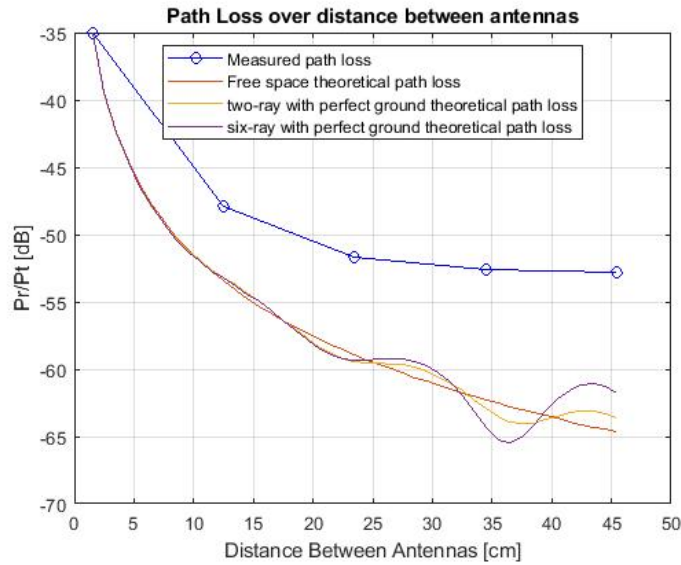


FIGURE 5.22: System path loss along distance without amplification

This is a uneven comparison of every model with our measurements. Free space model is impractical in an indoor situation, at least without an anechoic chamber which allows no reflections in the signal, which is completely different of our condition in the laboratory. Two-ray and six-rays models are also uneven to compare since they aim to predict path losses of distances of meters and above, which is not the case. That said, we can't directly compare the system path loss with the theoretical models, but we can see from Figure 5.22 that the greater distance, the smaller path loss which means that our received signal becomes weaker than at closer distances. This supports the idea that at close distances, the direct ray is so much stronger than the reflected rays that the reflected rays don't have a noticed effect on the path losses.

The best results obtained at the greater distance (Table 5.12) are very low considering the distance because the antenna gain is too low (around 2dB at 3.5 GHz). So, since we are obtaining EVM values close to -13dB and -14dB at such a small distance between the antennas, we decided to proceed and repeat the same tests but adding a signal amplifier to the system.

5.2.3 Amplified Wireless

5.2.3.1 Performance over Time

Since our BER is limited by the number of samples that AWG and DSO can operate to and record, each test can only carry 5 OFDM symbols. To understand how the system performance can vary over time, instead of transmitting more OFDM symbols, we need to repeat the realizations for, in this case, 20 times. So, Figures 5.23 and 5.24 show the variation of BER measured value, Mean BER over time and the total mean.

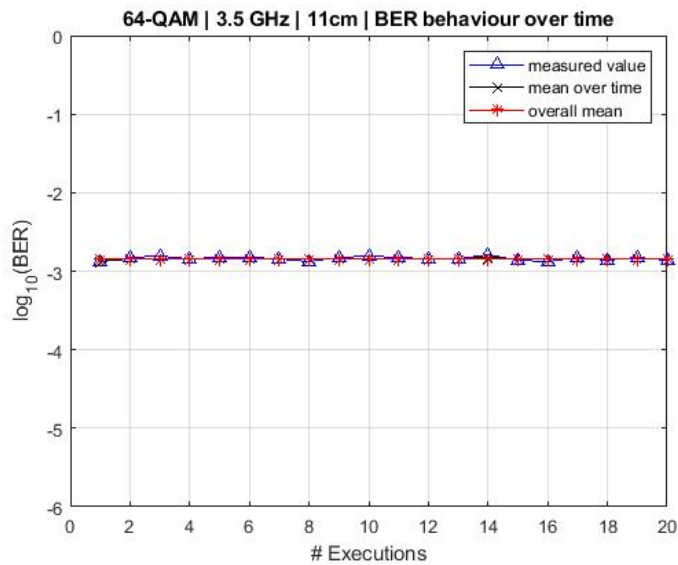


FIGURE 5.23: Variation of 64-QAM Uncoded BER over 20 realisations at 11cm distance

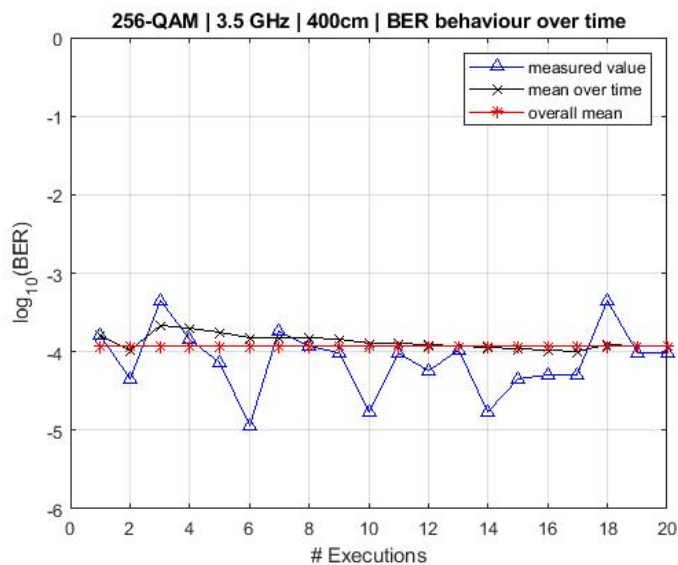


FIGURE 5.24: Variation of 256-QAM Hard Decision BER over 20 realisations at 400cm distance

Analysing Figures 5.23 and 5.24, we can conclude that for BERs above 1×10^{-3} the results are stable over time, which does not happen for 1×10^{-4} , 1×10^{-5} BER values. Although, the measured BER shows us that 20 realisations for same scenario in different time instants can give us a stable value when performing the calculation of Mean BER over time.

5.2.3.2 Performance along Distance

Figures 5.25 and 5.26 show, respectively, the EVM and BER performance along distance between antennas. With the amplifier, we managed to acquire distance results from 11cm to 400cm with consecutive gaps of 1 meter.

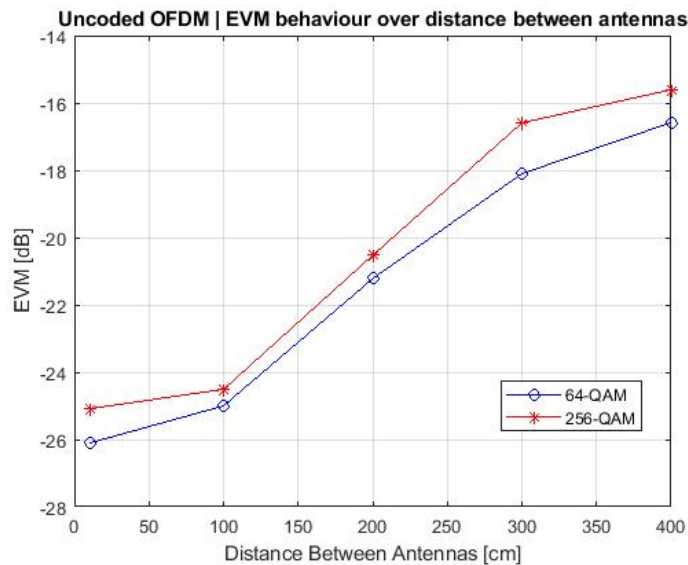


FIGURE 5.25: Uncoded 64/256 QAM EVM Performance along distance with amplification

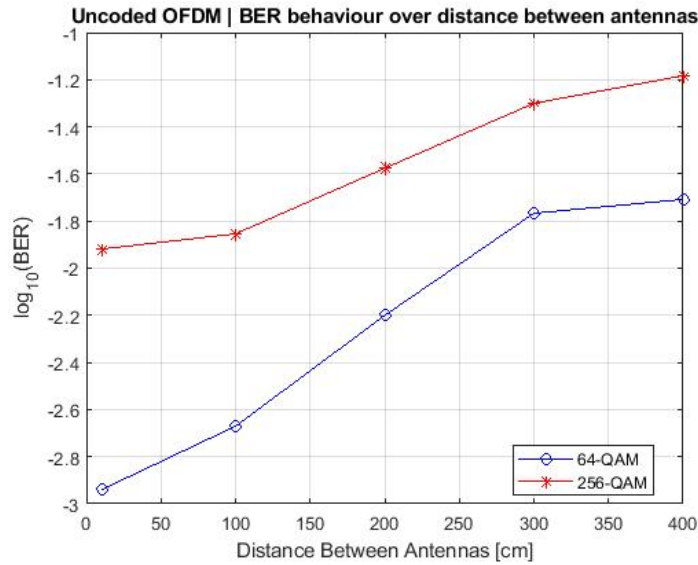


FIGURE 5.26: Uncoded 64/256 QAM BER Performance along distance with amplification

As expected, EVM and BER performances decrease with the increase of distance between antennas. From 11.0cm to 400.0cm EVM increases 8dB for 64-QAM and 9dB for 256-QAM and BER grows from 1.454×10^{-3} to 1.964×10^{-2} in 64-QAM and from 1.208×10^{-2} to 5.526×10^{-2} . EVM and BER performance show that it does not matter the order of the modulation, but the performance decrease from 11cm to 100cm and from 300cm to 400cm (around 1dB) is lower than the decrease across the middle distances which is around 4dB. The reason this is probably happening is that even though the antennas are 400cm distant from each other, the actual room is no bigger than 5m width. So the reflection on the back walls has an important effect since the signal became much stronger than it was in the remaining measurements. The path loss comparison will show that this effect is expected to happen. Tables 5.13, 5.14, 5.15, 5.16 and 5.17 show all the measurements made for each distance depending on QAM modulation order and the encoding scenario.

TABLE 5.13: BER Comparison between modulation and encoding scenarios for 11cm

Modulation	Encoding Scenario	EVM [dB]	Measured BER	Simulated BER
64-QAM	Uncoded	-26.1	1.454×10^{-3}	$< 1.782 \times 10^{-2}$
64-QAM	Hard Decision	-25.2	$< 7.632 \times 10^{-6}$	$< 5.581 \times 10^{-7}$
256-QAM	Uncoded	-25.1	1.208×10^{-2}	$< 1.516 \times 10^{-2}$
256-QAM	Hard Decision	-24.81	$< 5.724 \times 10^{-6}$	$< 1.603 \times 10^{-7}$

TABLE 5.14: BER Comparison between modulation and encoding scenarios for 100cm

Modulation	Encoding Scenario	EVM [dB]	Measured BER	Simulated BER
64-QAM	Uncoded	-25.0	2.149×10^{-3}	$< 1.782 \times 10^{-2}$
64-QAM	Hard Decision	-24.4	$< 7.632 \times 10^{-6}$	$< 5.581 \times 10^{-7}$
256-QAM	Uncoded	-24.5	1.397×10^{-2}	$< 1.516 \times 10^{-2}$
256-QAM	Hard Decision	-22.0	$< 5.724 \times 10^{-6}$	$< 1.603 \times 10^{-7}$

TABLE 5.15: BER Comparison between modulation and encoding scenarios for 200cm

Modulation	Encoding Scenario	EVM [dB]	Measured BER	Simulated BER
64-QAM	Uncoded	-21.2	6.311×10^{-3}	$< 1.782 \times 10^{-2}$
64-QAM	Hard Decision	-22.4	$< 7.632 \times 10^{-6}$	$< 5.581 \times 10^{-7}$
256-QAM	Uncoded	-20.5	2.680×10^{-2}	$< 1.516 \times 10^{-2}$
256-QAM	Hard Decision	-21.5	$< 5.724 \times 10^{-6}$	$< 1.603 \times 10^{-7}$

TABLE 5.16: BER Comparison between modulation and encoding scenarios for 300cm

Modulation	Encoding Scenario	EVM [dB]	Measured BER	Simulated BER
64-QAM	Uncoded	-18.2	1.717×10^{-2}	$< 1.782 \times 10^{-2}$
64-QAM	Hard Decision	-19.5	$< 7.632 \times 10^{-6}$	$< 5.581 \times 10^{-7}$
256-QAM	Uncoded	-16.6	4.982×10^{-2}	7.491×10^{-2}
256-QAM	Hard Decision	-17.5	1.145×10^{-5}	8.282×10^{-5}

TABLE 5.17: BER Comparison between modulation and encoding scenarios for 400cm

Modulation	Encoding Scenario	EVM [dB]	Measured BER	Simulated BER
64-QAM	Uncoded	-16.6	1.964×10^{-2}	2.719×10^{-2}
64-QAM	Hard Decision	-17.3	$< 7.632 \times 10^{-6}$	$< 5.581 \times 10^{-7}$
256-QAM	Uncoded	-15.6	6.526×10^{-2}	6.823×10^{-2}
256-QAM	Hard Decision	-13.2	1.202×10^{-4}	1.002×10^{-3}

As previously explained, the "less than" ($<$) signal is present and has the same meaning it had in the small distance results.

For larger distances, path loss models like two-ray and six-rays models are more suitable to compare to the measured results. Figure 5.27 shows the measured path loss values and the theoretical path losses of the same 3 different models presented in 2.6: free-space model, two-ray model with perfect ground ($\Gamma = -1$) and six-rays model with perfect ground (considering that the antennas are in the middle of the room, equally distant from the walls and with a clear LoS). The measured path loss is obtained by the subtraction of the received signal power (in dB) by the transmitted signal power (in dB).

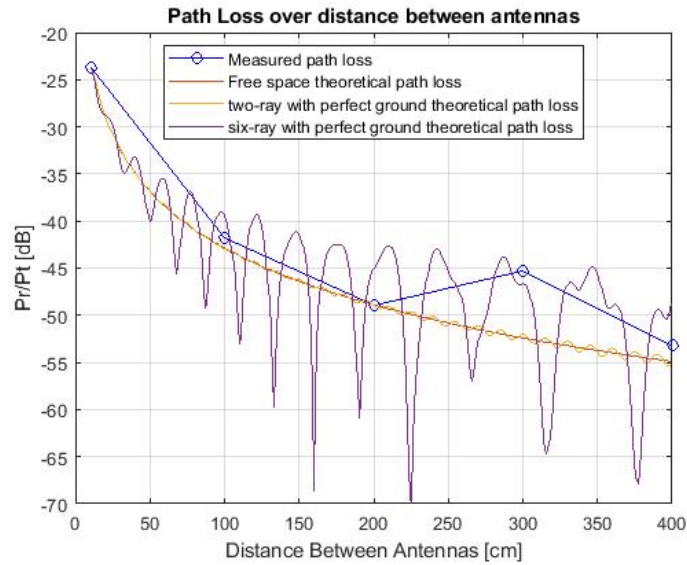


FIGURE 5.27: System path loss along distance with amplification

Note that comparing our system even to the six-rays model is a rough comparison, but is the closest one considering the experimental environment. The measured path loss seems to be accurate with the six-rays model with some fluctuation as expected. We can assume this is true because at the 300 cm distance we have an accentuated increase of signal strength than we had at 200cm which was also expected at the six-rays model. Overall the behaviour of our system is close to the six-rays model and this could only be improved by consequent amplifications and other experiment conditions. Unfortunately, it was not possible to acquire greater distance results because of the limited hardware and the small EVM needed to be improved to fit a real 5G system.

Chapter 6

Conclusions and Future Work

6.1 Conclusions

Considering all the presented work, there are some conclusions that the author would like to address and they are the following:

- Even though the simulator has some imperfections, it performed well and shows results that approximate the theoretical performances.
- The objective of studying and developing an high-rate transceiver is completed, the assumptions and specifications were the best within the time of execution of this dissertation.
- This study results in a 64-QAM OFDM 4.4Gbps effective data rate communication at 4 meters distance between antennas generating an EVM of -16.6 dB and a BER of 1.964×10^{-2} . This EVM value is still far from the -22.94 dB shown in Table 1.1.
- The best result was a 256-QAM OFDM 5.9 Gbps OFDM communication at 4 meters distance between antennas generating an EVM of -15.6 dB and a BER of 6.526×10^{-2} . This EVM value is still far from the -29.12 dB shown in Table 1.1 but is an achievable value considering further amplifications and signal enhancements.

6.2 Future Work

For future work, the authors would like to perform the following changes and improvements:

- Simulator should be reviewed to improve its performance and prevent non-linear effects in the generated signal.
- Simulator must have other types of equalizers and more powerful equalizers than ZF and MMSE equalizers, for example, the iterative equalizers which are more expensive in time and processing but, theoretically, the results are remarkably better.
- Further test should be made with a ray tracing tool to understand how the signal strength should vary inside the laboratory.
- Simulation and experimental realizations considering more powerful FECs, as soft decision convolutional codes, Low-density Parity-Check Codes (LDPC), TCH Codes and other.
- A complete study of the experimental system and hardware selection and testing to improve the signal strength and hopefully test the transmissions at distances above 10 meters outdoor.

Bibliography

- [1] E. Mohyeldin, “Minimum Technical Performance Requirements for IMT-2020 radio interface(s),” *Workshop on IMT-2020 terrestrial radio interfaces*, p. 12, 2017.
- [2] M. Tan and W. Chen, “Performance comparison and analysis of PSK and QAM,” *7th International Conference on Wireless Communications, Networking and Mobile Computing, WiCOM 2011*, pp. 0–3, 2011.
- [3] K. Technologies, “First Steps in 5G,” tech. rep., USA, 2019.
- [4] A. R. James, R. S. Benjamin, S. John, T. M. Joseph, V. Mathai, and S. S. Pillai, “Channel estimation for OFDM systems,” *2011 - International Conference on Signal Processing, Communication, Computing and Networking Technologies, ICSCCN-2011*, no. Icscn, pp. 587–591, 2011.
- [5] F. D. Stasio, M. Mondin, and F. Daneshgaran, “Multirate 5G Downlink Performance Comparison for f-OFDM and w-OFDM Schemes with Different Numerologies,” *2018 International Symposium on Networks, Computers and Communications (ISNCC)*, pp. 1–6.
- [6] C. An, B. Kim, and H. G. Ryu, “Design of W-OFDM and nonlinear performance comparison for 5G waveform,” *2016 International Conference on Information and Communication Technology Convergence, ICTC 2016*, pp. 1006–1009, 2016.
- [7] P. Naga Rani and C. H. Santhi Rani, “UFMC: The 5G modulation technique,” *2016 IEEE International Conference on Computational Intelligence and Computing Research, ICCIC 2016*, pp. 1–3, 2017.
- [8] C. Balint, “OFDM-Based Multi-Carrier Waveforms Performances in 5G,” *2018 International Symposium on Electronics and Telecommunications (ISETC)*, pp. 1–4, 2018.

- [9] X. Yang, X. Wang, and J. Zhang, "A New Waveform based on Slepian Basis for 5G System," *2016 Wireless Days (WD)*, pp. 1–4, 2016.
- [10] A. Hazareena, "A SURVEY : ON THE WAVEFORMS FOR 5G," *2018 Second International Conference on Electronics, Communication and Aerospace Technology (ICECA)*, no. Iceca, pp. 64–67, 2018.
- [11] H. Wang, A. A. Zaidi, X. Chen, J. Luo, and M. Dieudonne, "Evaluation of 5G Waveform Candidates Considering Hardware Impairments and above 6 GHz Operation," *IEEE Vehicular Technology Conference*, vol. 2017-June, no. 1, 2017.
- [12] P. Weitkemper, J. Koppenborg, J. Bazzi, R. Rheinschmitt, K. Kusume, D. Samardzija, R. Fuchs, and A. Benjebbour, "Hardware experiments on multi-carrier waveforms for 5G," *2016 IEEE Wireless Communications and Networking Conference Workshops, WCNCW 2016*, no. Nwm5g, pp. 270–275, 2016.
- [13] J. Bazzi, P. Weitkemper, K. Kusume, A. Benjebbour, and Y. Kishiyama, "Design and Performance Tradeoffs of Alternative Multi-Carrier Waveforms for 5G," *2015 IEEE Globecom Workshops (GC Wkshps)*, pp. 1–6, 2015.
- [14] M. L. J. Vora, "Evolution of Mobile Generation Technology : 1G To 5G and Review of Upcoming Wireless Technology 5G," *Scientific Journal Impact Factor*, vol. 2, no. 10, pp. 281–291, 2015.
- [15] B. R. W. Chang, "Synthesis of band-limited orthogonal signals for multi-channel data transmission," 1966.
- [16] R. W. Chang, "Orthogonal Frequency Multiplex Data Transmission System," 1970.
- [17] M.-G. D. Benedetto and G. Giancola, *Understanding ultra wide band radio fundamentals*. Upper Saddle River, N.J.: Prentice Hall PTR, 2004.
- [18] S. B. Weinstein and P. M. Ebert, "Data Transmission by Frequency-Division Multiplexing Using the Discrete Fourier Transform," *IEEE Transactions on Communication Technology*, vol. 19, no. 5, pp. 628–634, 1971.
- [19] R. van Nee and R. Prasad, *OFDM Wireless Multimedia Communications*. Norwood, Massachusetts: Artech House Publishers, 2000.

- [20] W. Shieh and I. Djordjevic, *Orthogonal Frequency Division Multiplexing for Optical Communications*. Elsevier Science Publishing Co Inc, 2010.
- [21] Ericsson, Nokia, Motorola, and Rohde & Schwarz, “Proposal for LTE channel models,” in *TSG-RAN Working Group 4 (Radio) meeting*, p. 7, 2007.
- [22] J. H. Lodge and M. L. Moher, “Time diversity for mobile satellite channels using trellis coded modulations,” *IEEE Global Telecommunications Conference, Tokyo, Japan*, vol. 1, pp. 303–307, 1987.
- [23] J. K. Cavers, “An analysis of Pilot Symbol Assisted Modulation for Rayleigh Fading Channels,” *IEEE Trans. Veh. Technol.*, vol. 40, no. 4, pp. 686–693, 1991.
- [24] N. Souto, *Turbo-processing Techniques for WCDMA Systems*. PhD thesis, Universidade Técnica de Lisboa- Instituto Superior Técnico, 2006.
- [25] B. Farhang-Boroujeny, “Pilot-based channel identification: A proposal for semi-blind identification of communication channels,” *Electron. Lett.*, vol. 31, no. 13, pp. 1044–1046, 1995.
- [26] O. Landron, M. J. Feuerstein, T. S. Rappaport, and S. Member, “A Comparison of Theoretical and Empirical Reflection Coefficients for Typical Exterior Wall Surfaces in a Mobile Radio Environment,” vol. 44, no. 3, 1996.
- [27] C. Sommer, S. Joerer, and F. Dressler, “On the Applicability of Two-Ray Path Loss Models for Vehicular Network Simulation,” *2012 IEEE Vehicular Networking Conference (VNC)*, pp. 64–69, 2012.
- [28] J. R. Costa, C. R. Medeiros, C. A. Fernandes, and S. Member, “Performance of a Crossed Exponentially Tapered Slot Antenna for UWB Systems,” vol. 57, no. 5, pp. 1345–1352, 2009.